Sustained store-operated calcium entry utilizing activated chromatin state leads to instability in iTregs

Author

Huiyun Lyu[1,2#], Guohua Yuan[3,4#], Xinyi Liu[1,5], Xiaobo Wang[1,5], Shuang Geng[6], Tie Xia[1,5], Xuyu Zhou[7,8], Yinqing Li[3,4], Xiaoyu Hu[1,2,5], Yan Shi[1,2,5,6*]

Affiliations

[1]Institute for Immunology, Beijing Key Lab for Immunological Research on Chronic Diseases, Tsinghua University, 100084, Beijing, China.

[2]Tsinghua-Peking Center for Life Sciences, Tsinghua University, 100084, Beijing, China.

[3]IDG/McGovern Institute for Brain Research and School of Pharmaceutical Sciences, Tsinghua University, 100084, Beijing, China.

[4]MOE Key Laboratory of Bioinformatics, Center for Synthetic and Systems Biology, School of Pharmaceutical Sciences, Tsinghua University, Beijing, P. R. China.

[5]Department of Basic Medical Sciences, School of Medicine, Tsinghua University, 100084, Beijing, China.

[6]Department of Microbiology, Immunology and Infectious Diseases, Snyder Institute, University of Calgary, Calgary, Alberta, Canada.

[7]Key Laboratory of Pathogenic Microbiology and Immunology, Institute of Microbiology, Chinese Academy of Sciences, Beijing 100101, China.

[8]University of Chinese Academy of Sciences, Beijing 100049, China.

[#]These authors contributed equally

[*]Correspondence: Yan Shi, D301 Medical Sciences Bldg, Tsinghua University, 100084, Beijing, China yanshiemail@mail.tsinghua.edu.cn

Abstract

Thymus-originated tTregs and *in vitro* induced iTregs are subsets of regulatory T cells. While they share the capacity of immune suppression, their stabilities are different, with iTregs losing their phenotype upon stimulation or under inflammatory milieu. Epigenetic differences, particularly methylation state of Foxp3 CNS2 region, provide an explanation for this shift. Whether additional regulations, including cellular signaling, could directly lead phenotypical instability requires further analysis. Here we show that upon TCR triggering, store-operated calcium entry (SOCE) and NFAT nuclear translocation are blunted in tTregs, yet fully operational in iTregs, similar to Tconvs. On the other hand, tTregs show minimal changes in their chromatin accessibility upon activation, in contrast to iTregs that demonstrate an activated chromatin state with highly accessible T cell activation and inflammation related genes. Assisted by several cofactors, NFAT driven by strong SOCE signaling in iTregs preferentially binds to primed opened T helper (T_H) genes, resulting in their activation normally observed only in Tconv activation, ultimately leads to instability. Conversely, suppression of SOCE in iTregs can partially rescue their phenotype. Thus our study adds two new layer, cellular signaling and chromatin accessibility, of understanding in Treg stability, and may provide a path for better clinical applications of Treg cell therapy.

Introduction

The regulatory T cells (Tregs) are key to maintain peripheral immune tolerance and to block excessive inflammatory reactions. There are two main populations of Tregs. The prototypical one originates from the thymus (tTreg), sharing a developmental program similar to conventional T cells [1,2]. Their TCRs are believed to have higher basal affinity to MHC, and express Foxp3 during CD4 single positive period [3]. The other population originates from the periphery (pTregs) via conversion of Tconvs, arising during inflammation with proper antigenic stimulation and inductive cytokine environment [4–6]. iTregs, mimicking the induction of pTregs, is a type of Tregs induced *in vitro* in the presence of TGF-β [7,8]. While iTregs share similarity in suppressive capacities to Tregs *in vivo* [9–11], they are different from tTregs in several aspects, particularly regarding their stabilities. Although tTregs in some occasions show certain levels of plasticity, their phenotypes are mostly stable, both *in vivo* and *in vitro* [12]. iTregs induced *in vitro* are more labile with marked loss of Foxp3 expression after activation, limiting the duration of their suppression [13,14]. The short life of iTregs is also a roadblocker of the clinical use of Treg cell therapy, as they cannot be used as an alternative source to replace numerically limited tTregs [15]; and in cases where iTregs are raised with targeted specificities, they carry concerns of potential self-reactivity following the loss of Foxp3.

The stability of tTregs is established prior to their exit from the thymus [16]. In the thymus, Foxp3 works with other transcription factors, such as NFAT and c-Rel to maintain a steady transcriptional program [17–19]. At the same time, the extensive demethylation of FoxP3 CNS2 is also critical to their stable phenotype, an event likely taking place before FoxP3 expression [19,20]. While epigenetic differences provide a possible explanation of Treg stability, it is more probable that multiple factors collectively contribute to the difference. Unlike Tconvs that undergo expansion, attrition and memory states after activation, tTregs lose signature changes and return to their original state following activation [21]. This persistence in phenotype of tTregs is certainly beneficial to the host, yet mechanisms for this maintenance, in contrast to the lack thereof in iTregs are incompletely understood. Previous work suggests that TCR signal as well as ensuing Ca^{2+} activities are weaker in tTregs [22–24], whether the reduced TCR signaling strength is the root of tTreg stability remains an intrigue, particularly strong TCR engagement facilitates iTregs' loss of phenotype.

Here we report a surprising finding that may contribute to the iTregs' phenotypical change after their activation. We found that ligation of TCR induces long vibration of Ca^{2+} signals in Tconvs that lasts for hours, as typically expected in the SOCE activation. Initially similar, this vibration is quickly diminished in tTregs, correlating with their reduced response to TCR stimulation. In contrast, in iTregs, this Ca^{2+} vibration is indistinguishable from Tconvs. The sustained Ca^{2+} signal leads to a strong NFAT activation in iTregs. Regarding chromatin accessibility, with the aid of our initial observation of iTregs

from the perspective of activated Tconv, we found iTregs also show an "activated" chromatin state with T cell activation and inflammation related genes highly open. We demonstrate that the NFAT nuclear translocation driven by sustained calcium signal allows its direct access to prime-opened T_H genes and upregulate their expression, destabilizing iTregs. As expected, blocking CRAC channel reverses the loss of FoxP3 in iTregs *in vitro* and *in vivo*. Our work therefore suggests that Ca^{2+} signaling and accessible chromatin state in iTregs are two key causes in their loss of stability following activation, which may be of important value to understand how these two populations of Tregs operate in the disease conditions and lead to better applications of iTregs in the clinic.

Results

iTregs use a suppression mechanism similar to that of tTregs

In our previous work, we found that Tregs show strong binding to DCs, which is a key mechanism for blocking DC's ability to engage other Tconvs [25]. The strong binding is due to low basal calcium oscillation of tTregs in the steady state [26], which leads to diminished mCalpain activation and commensurate reduced internalization of LFA-1. Furthermore, our previous study showed the low calcium oscillation is maintained by reduced expression of endosomal Ca^{2+} channel Ryr2 by Foxp3 [26]. To ascertain that this regulation is also central to iTregs, we produced iTregs from Tconvs. With plate bound anti-CD3/CD28 and in the presence of TGF-β, iTregs were induced and the percentage was maximized on day 2. We found that *in vitro* iTregs show stronger suppression than tTregs on OT-II proliferation in response to epitope peptide loaded DCs (Fig 1A). In accordance with the stronger suppression, single cell force spectroscopy analysis showed that iTregs possessed apparent binding to DCs, even stronger than tTregs (Fig 1B). In addition, iTregs also showed increased binding force compared with activated Tconvs (Fig 1C), suggesting the strong binding force is a common feature of both types of Tregs, but not Tconvs. We measured the expression of FoxP3 more precisely, and noticed that the protein level expression of FoxP3 reached its peak on day 2 after the induction (Fig 1D). With the accumulation of FoxP3 protein, basal Ca^{2+} oscillation in the treated Tconvs was gradually diminished, with the former leading the latter roughly by one day (Fig 1E). As expected, the transcription level of Ryr2 was suppressed both in iTregs and tTregs (Fig S1A), suggesting that the strong binding force with DC may come from reduced calcium oscillation as a result of FoxP3-mediated suppression of Ryr2 transcription. While Ryr2 expression may be regulated by Foxp3, the induction efficiency of Foxp3 was not affected by Ryr2 knock out (Fig S1B). Therefore, we show iTregs can apply a suppression mechanism similar to tTregs, which operates via the indirect inhibition via DC blockage. We do not know why iTregs show a stronger suppression than tTregs, an event maybe related to their activation in the induction process.

112

113 **Sustainment of SOCE and NFAT nuclear translocation are reduced in tTregs, but not in iTregs**

114 It was reported previously that TCR signaling led to a dramatic reduction of FoxP3+ cells in iTregs,
115 but not in tTregs [14,27]. We reproduced this data in our lab (Fig 2A). tTregs have been reported to show
116 an attenuated response to TCR triggering [22–24], the exact point of signal attenuation in tTregs has not
117 been elucidated. In immune cells, there are mainly three types of Ca^{2+} signals, the steady state low
118 level Ryr2-based membrane proximal Ca^{2+} "puff"; the TCR ligation-triggered, inositol triphosphate-
119 mediated IP3R opening on the ER membrane; and ER Ca^{2+} depletion-induced, sustained Ca^{2+} influx
120 upon SOCE activation [28]. As the extracellular Ca^{2+} is roughly 4 logs higher than the intracellular,
121 SOCE activation is by far the strongest Ca^{2+} event in T cells (Fig S2A), and is also distinct from the
122 other Ca^{2+} signaling patterns for its persistent vibration lasting hrs to days [29,30].

123 We wondered if the reported TCR signal truncation in tTregs was manifested as reduced SOCE
124 activities. We titrated anti CD3/CD28 concentrations, and iTregs lost Foxp3 at the lowest dose
125 required to activate, yet tTregs were resistant to an 8-fold increase in both (Fig S2B). To study the
126 molecular basis for the weak response in tTregs, we first monitored the early SOCE intensity in iTregs
127 and tTregs, we found the first wave of SOCE in iTregs was slightly higher than Tconvs and tTregs, but
128 there was no discernable difference between tTregs and Tconvs (Fig 2B). In addition, the
129 phosphorylation of CD3ζ was similar in Tconv and nTreg immediately after TCR crosslink (Fig S2C).
130 As full T cell activation requires sustained SOCE activation [31], we extended the observation time
131 window. As SOCE signal is synchronized upon initial TCR trigger, each individual T cell SOCE
132 oscillation hours into activation is no longer in unison [29,32], we therefore recorded Ca^{2+} waves in
133 individual cells. In Tconvs and iTregs, Ca^{2+} remained cyclic waves expected in SOCE pulsation. In
134 contrast, this Ca^{2+} signal was suddenly lost in tTregs 40-50 min after the activation (Fig 2C) (Movie
135 1-3).

136 In contrast to other transcriptional factors, such as NF-κB, activated rapidly in response to short Ca^{2+}
137 elevation, NFATs are known to be triggered only by sustained cytoplasmic Ca^{2+} [31,33,34]. Indeed, in
138 contrast to iTregs and Tconvs, tTregs' NFATc1 and c2 failed to translocate into the nucleus (Fig 2D).
139 Upon detailed analysis, in iTregs, anti-CD3/CD28 stimulation led a quick drop in cytoplasmic NFAT
140 in two hours, with moderate accumulation of NFAT in the nucleus (Fig S2D). This was followed by
141 continuous synthesis of NFAT in the cytoplasm and accumulation of nuclear NFAT [35,36]. While tTregs
142 are known to have reduced NFAT activation in response to TCR ligation [22,37], our results pointed to a
143 truncated Ca^{2+} response likely to be the molecular basis for this phenotype. With this association
144 potentially established, we wondered if the length of SOCE itself is sufficient to explain the stability
145 difference between iTregs and tTregs. Non-specific Ca^{2+} membrane permeability modifier such as

146 ionomycin resulted in large scale cell death (Fig S2E), we therefore used SERCA inhibitor
147 Thapsigargin (TG). Blocking SERCA leads to endosome Ca^{2+} reloading blockage that leads to
148 continuous translocation of STIMs to the plasma membrane-ER junction and Orai channel opening.
149 In contrast to indiscriminating Ca^{2+} overload, pure SOCE activation was not followed by significant
150 cell death (Fig S2E). As expected, some tTregs treated with TG lost their Foxp3 (Fig 3E). These results
151 collectively argue that the truncated Ca^{2+} in tTregs is essential to protect tTregs from phenotypical
152 shift.
153
154 **iTregs display activated chromatin state with highly open activation region**
155 As shown, the behaviors of SOCE signaling and NFAT of iTregs were closer to their precursor
156 Tconvs rather than tTregs, we were curious about the systemic similarity among iTregs, Tconvs and
157 tTregs. Therefore, we performed RNA-seq and Assay for Transposase-Accessible Chromatin with
158 high-throughput sequencing (ATAC-seq) of iTregs, together with resting/activated tTregs and
159 Tconvs.
160 In RNA-seq data, principal component analysis (PCA) and heatmap of DEG indicated that Tconvs
161 were quite different before and after activation, but the changes of tTregs before and after TCR
162 activation were more limited compared with Tconvs (Fig 3A and Fig S3C), verifying that tTregs have
163 low TCR responsiveness. Comparing the transcriptome characteristics with other cell types, iTregs
164 acquired partial Treg features after induction, shown as an intermediate between Tconvs and tTregs
165 on PC2 (Fig 3A and Fig S3B). While among all cell states, iTregs had the highest PC1 scores,
166 represents higher proliferation state, probably due to the 4 days of induction (Fig 3A and Fig S3A).
167 Next, we analyzed the chromatin accessibility of these cells using ATAC-seq data. In the PCA plot,
168 tTregs showed fewer changes after activation compared to Tconvs, while iTregs were closer to
169 activated Tconv cells (Fig 3C). In differential peak heatmap clustered by cell type, Tconvs became
170 more accessible in "Activation Region" after activation, and with a dramatic increase in the overall
171 accessibility (Fig 3C). However, the changes of tTregs after activation are limited, the majority of
172 tTreg-specific accessible region, named "Treg Region", were not changed. Also the activation region
173 opening seen in Tconvs were not more accessible in tTregs (Fig 3C). All of these characteristics
174 indicated that tTreg phenotype is highly ensured by their low TCR responsiveness which potentially
175 led to their refusal to change chromatin accessibility seen in Tconvs following activation.
176 When comparing iTregs with the others, we found iTregs were highly accessible in activation region
177 found in activated Tconvs (Fig 3C and Fig 3D). However, only a few Treg specific peaks shown in
178 Treg region were opened in iTregs (Fig 3C and Fig 3E). For further analysis, we isolated Treg
179 specific peaks. It was clear that most of them were opened in tTregs but showed little accessibility in

180 iTregs (Fig S3D). For example, Foxp3 and Ctla4, expressed in both tTregs and iTregs, show high
181 accessibility in resting and activated tTregs, but were closed or only partially opened in iTregs (Fig
182 3G). In contrast, genes related to inflammation cytokine in T helper cells, such as Ifng, Il4, Il17ra
183 and Il21, were highly opened in iTregs (Fig 3F). In further elaboration of Activation Region in
184 Figure 3D, we have selected some genes including typical peaks that are within this region (Fig S3E).
185 These genes encompass some T-cell activation-associated transcription factors, such as Irf4, Atf3, as
186 well as multiple members of the Tnf family including Lta, Tnfsf4, Tnfsf8, and Tnfsf14. Additionally,
187 genes related to inflammation cytokine and function such as Il12rb2, Il9, and Gzmc are included.
188 These genes display elevated accessibility upon T-cell activation, partially open in activated tTreg
189 cells. However, all of them exhibit high accessibility in iTreg cells.
190 Overall, we showed that at the gene expression level, iTregs have acquired some Treg features, but
191 the chromatin accessibility was mostly trapped in activated Tconv state, not only with regard to the
192 closed Treg genes, but also with genes associated with T activation and inflammation highly opened.
193 The latter is expected to be mainly closed in genuine Tregs in accordance with their lower
194 responsiveness to TCR triggering. We speculate that this "unconverted" chromatin accessibility,
195 especially the highly opened activated genes will contribute to iTreg instability upon TCR
196 stimulation. It is therefore interesting whether NFAT accumulated in nuclei driven by sustained
197 calcium oscillation will indeed target those genes for an activation state unfit for their phenotypical
198 stability.
199
200 **SOCE and NFAT directly leads to phenotypical instability in iTregs**
201 To further validate the role of calcium and NFAT in iTreg instability, we used inhibitors cyclosporine A
202 (CsA) and CM-4620 to suppress calcium signal and NFAT, respectively. We found that inhibition of
203 calcium or NFAT rescued the Foxp3 expression in iTregs upon restimulation (Fig 4A). Another SOCE
204 inhibitor BTP2 was also verified (Fig S4A). Accordingly, ionomycin, which can directly induce
205 calcium release independent of TCR activation, also lead to iTreg instability (Fig S4B). Thus, NFAT
206 and calcium signaling blockage was correlated to iTreg stability. As control, inhibition of NFkB (BAY
207 11-7082), c-Jun (SP600125), or a c-Jun/c-Fos complex (T5224) had no discernable effect, or in one
208 case, possibly further reduction in stability (Fig S4C). These results may indicate that NFAT plays a
209 crucial and special role in TCR activation, which leads to iTreg instability.
210 To investigate how NFAT and calcium signaling destabilize iTregs, we performed RNA-seq on these
211 cells. From the differential gene expression and principal component analysis, we found that iTregs
212 upon restimulation showed significant differences from the resting state at the transcriptome level, and
213 this difference could be substantially reduced with inhibition of calcium or NFAT (Fig 4B). As shown

214 in the PCA plot, calcium/NFAT-blocked iTregs were significantly closer to the resting state than the
215 unstable ones (Fig 4C). Thus, inhibition of calcium or NFAT can significantly improve the stability of
216 iTregs as reflected by transcriptomic identity. In addition, the large overlap (about 80%) of genes that
217 were rescued by CM-4620 and by CsA further supported that calcium signaling change the fate of
218 iTregs mainly through NFAT (Fig 4D).
219 Among the genes rescued by CM-4620 and CsA, they can be further divided into two groups.
220 Members of the first group were downregulated upon restimulation and the downregulation was
221 blocked by inhibition of calcium and NFAT. This result indicating that these genes are downregulated
222 by NFAT. Among these genes, several of them are critical for functions and stability of Tregs, such as
223 Foxp3, Id3, Il10rb, Sema4a, Tgfbr1/2, Ms4a4b, Nlrp6 (Fig 4B and Fig S4D). In the functional analysis
224 of these genes, we found that Rap-1 pathway, PD-1/PD-L1 pathway and Foxo pathway were
225 significantly enriched (Fig S4E). Loss of these genes was therefore consistent with the phenotype of
226 iTreg instability.
227 The other group had genes that were otherwise upregulated after restimulation, but failed to do so with
228 CM-4620 or CsA, indicating that these genes are upregulated by NFAT. In these genes, many of them
229 are associated with T helper differentiation and T cell activation, such as Il21, Il12rb2, Tbx21, Gzma,
230 Stat2, Stat3, Atf3, Fasl (Fig 4B and Fig 4F). Among them, Il21 encodes a key cytokine in Th17
231 differentiation, Tbx21, encoding T-bet, and Il12rb2 are key transcriptional factors and cytokine
232 receptor for Th1 differentiation. Functional enrichment analysis of these upregulated genes pointed to
233 Th17 related pathway and Th1/Th2 related pathways (Fig 4E). Further validation of these upregulation
234 T helper related genes (T_H genes) by NFAT was perform by QPCR (Fig 4G). These results in all
235 indicated the iTreg restimulation was associated with a strong tendency of differentiation towards
236 non-Treg polarization, and NFAT was likely a key regulator in this process.
237
238
239 **NFAT upregulate prime-opened T_H genes to destabilize iTregs**
240 To further study the role of NFAT in iTreg instability, we performed Cut&Tag assay to acquire the
241 NFAT binding sites in resting iTregs and those after restimulation (Fig 5A). NFAT-flag and
242 anti-Flag antibody was used to capture peaks that were bound by NFAT (Fig S5A). The binding
243 peaks were of high quality as indicated by the lower number of peaks in the mock control compared
244 to both resting and activated states (Fig 5B). The number of NFAT peaks in restimulated iTregs was
245 significantly higher than that in resting state, which was consistent with the massive nuclear
246 translocation of NFAT indicated by western blot (Fig 5B and Fig 2D). For peak distribution at gene
247 body, NFAT peaks both before and after restimulation were enriched at promoters/TSS and the first

248 introns of genes (Figures S5C).
249 For those upregulated T_H genes, we speculated that this may be associated with the highly "activated"
250 chromatin state of iTregs mentioned earlier. Therefore, we first checked the chromatin accessibility
251 around the transcription start site (TSS) in those genes and found that this group of genes was
252 significantly more accessible in iTregs than in tTregs and Tconvs (Fig 5C). As shown in the genome
253 browser view, Il21, Il12rb2 and Tbx21 were more open in iTregs, even more so than the activated
254 Tconvs (Fig S5B). Further analysis revealed that NFAT significantly increased their binding to the
255 TSS regions on upregulated Th genes after restimulation (Fig 5D), while showing little change on
256 downregulated Treg genes (Fig 5SD). As shown by Il21, Tbx21 and Il12rb2, after activation, NFAT
257 accumulated at the sites that were prime-opened resulting in their increased expression (Fig 5E).
258 Therefore, the enhanced chromatin accessibility revealed in Fig 4 was indeed approached by the
259 large amount of NFAT, leading to T cell polarization towards other directions with a sole reciprocal
260 loss of polarization towards Tregs. This tendency may to some extent explain the rapid loss of iTreg
261 phenotype.
262 As one potential counter argument, NFAT is ostensibly essential to the development of tTregs [38,39].
263 In the induction of iTregs, NFAT in collaboration with SMAD is also critical [23,39,40]. It is therefore
264 intriguing why NFAT re-activation after iTreg formation may serve as a key factor in compromising
265 iTreg stability. To resolve those seemingly contradictory regulations, we performed NFAT motif
266 enrichment analysis. The results showed that putative BATF, AP-1(Fos/Jun), RORg binding sites
267 were highly enriched in restimulation state specific regions (Fig 5F). For the preference of different
268 co-factors to different gene subsets, SMAD family tended to bind to genes that were downregulated
269 by NFAT, for example, Foxp3, while AP-1 and RORg preferred binding to genes that were
270 upregulated by NFAT, such as T_H genes (Fig. 5G). Taken together, our results appear to suggest that
271 upon restimulation of iTregs, NFAT prefers to cooperate with AP-1/RORg to promote the expression
272 of prime opened T_H gene expression, and at the same time denies the SMAD programming that may
273 be critical to maintain Treg functions and stabilities. Certainly, how much this selective cooperation
274 between NFAT and other transcriptional factors contributes to iTreg instability remains speculative
275 until large scale ChIP-seq analyses are performed on the players involved.
276 According to the Cut&Tag data, the secretion levels of IL-21 in tTreg and iTreg was also examined by
277 ELISA. As shown in Fig 5H, tTreg did not secrete IL-21 regardless of activation status (undetectable),
278 while iTreg did not secrete IL-21 at resting state but they did so after 48 h of restimulation. The
279 secretion of IL-21 was inhibited by CsA and CM-4620 treatment. This observation aligns with our
280 findings where nuclear binding of NFAT to gene loci of these cytokines enhanced their expression,
281 pushing iTreg unstable under inflammatory conditions. These findings further underscore the

likelihood that the inhibition of calcium and NFAT signaling might contribute to the stabilization of iTreg by suppressing the secretion of inflammatory cytokines.

Reduction of SOCE enhances iTreg stability and suppressive potential

Given that sustained calcium signal and NFAT translocation can directly disrupt iTreg stability, we asked whether manipulation of calcium signaling or NFAT can conversely be used to stabilize those cells. As Treg suppression assays require the participation of other T cells which are sensitive to inhibitory agents added indiscriminately, after regular iTreg induction, we overexpressed a dominant negative ORAI (DN-ORAI), whose single monomer incorporation will lead to a functionally disabled ORAI hexamer, to control the SOCE signal upon iTreg restimulation [41]. As expected, the mutated ORAI reduced the SOCE signaling by about a half (Fig 6A). When we restimulated this DN-ORAI expressing iTregs with anti-CD3/CD28, they showed stronger stability with higher retention of Foxp3 than WT-ORAI iTregs (Fig 6B). Consistently, DN-ORAI iTregs displayed more potent suppressive activity than control iTreg in *in vitro* suppression assay (Fig 6C).

Finally, the stability of DN-ORAI iTregs *in vivo* was examined. In brief, OT-II iTregs were infected with DN-ORAI retrovirus and then purified by GFP fluorescence, then the CD45.2^{+} GFP^{+} Foxp3-RFP^{+} iTregs were adoptively transferred into CD45.1 recipient, and OVA/Alum were administrated to restimulate DN-ORAI iTregs *in vivo*. Analysis of the percentage of Foxp3^{+} cells in mLN 5 days after adoptive transfer showed that DN-ORAI iTregs were more resistant to the loss of Foxp3 and thus were more stable than control WT-ORAI iTregs (Fig 6D). These results collectively showed that weakened calcium signal and inhibition of NFAT can quantitatively prevent iTregs from losing more Foxp3 both *in vitro* and *in vivo*, thus permitting a stronger suppressive capacity and a longer stability.

Based on extensive opening of activation regions approached by NFAT in the process iTreg stimulation, we postulate that openness of activation region could be another crucial feature of Treg stability, in addition to closed Treg region by low TSDR. Beyond the basal regimens of anti-CD3, anti-CD28, IL-2, and TGF-β, several additional factors have been reported to enhance the stability of iTregs, including the use of retinoic acid, rapamycin, vitamin C, and AS2863619 as well as removal of CD28 signaling[42–46]. We observed if those new additions in some ways altered the state of TSDR as well as the the openness of activation region. Our findings revealed that Rapamycin and AS tended to close the activation region (Fig S6A), while Vc, removal of CD28, and AS increased the accessibility of Treg genes (Fig S6B). These results indicate that different treatments have varied impacts on the activation region and Treg region. Hence the selective and combinatorial use of those factors is an interesting proposal in the generation of more stable iTregs.

Discussion

tTregs are different from other subsets of CD4 T cells in the thymic determination of their phenotype. To some extent, this centric determination is closer to CD4/CD8 demarcation, rather than other polarizations in the peripheral environment [1,2]. The stable phenotype, even after activation, is critical to provide the baseline immune suppression [12]. pTregs/iTregs are driven by the environment. It is logical that those cells should be deprived of their suppressive ability when are no longer needed to avoid unnecessary accumulation of those cells. The current understanding is that during thymic development, FoxP3 CNS2 region is selectively demethylated, allowing several transcriptional factors, such as Ets1 and FoxP3 itself to binding to this location [19,20]. This is one of several epigenetic features that maintain the stability, and TCR signaling in tTregs does not change the pre-established hypomethylation state. Induced Tregs, on the other hand, use a different program that relies on the binding of SMADs to the CNS1 region to initiate FoxP3 expression [40]. This SMAD binding mediated transcription is dependent on Foxp3 H3K4me3 modification. In the absence of SMAD, H3K4me3 is partially lost, resulting in iTreg phenotypical shift [40]. Withstanding this paradigm, iTregs do not immediately lose FoxP3 expression upon TGF-β withdrawal, the loss of FoxP3 is evident hours or days after TCR signaling [27]. This indicates that while the epigenetic alterations are necessary, an activation event is required to drive the loss of phenotype. This notion is subtly echoed by the limited TCR signaling in tTregs, implying that the hypo responsiveness to TCR ligation may be a critical feature to maintain their stability.

We observed differences between tTregs and iTregs in calcium signal and Th gene accessibility. tTregs utilize both truncated calcium signal and conserved chromatin accessibility to systematically reduce their TCR responsiveness, ensuring their stability. In contrast, iTregs retain the full strength of the TCR signaling, particularly the sustained vibration of SOCE signal, the key factor that drives NFAT synthesis and nuclear translocation. With the help of several cofactors, such as AP-1, NFAT caused the high expression of these T_H genes, which subsequently subverts the original differentiation of iTregs, leading to their instability. Direct inhibition of SOCE signaling and NFAT can enhance iTreg stability *in vitro* and *in vivo* (Fig 6E).

Previous observations also showed that the calcium signal in tTreg is weaker than that in Tconvs, and NFAT activity is suppressed in tTregs. The weaker Ca^{2+} signal in previous reports was seen as early as 10 min into activation, this contradiction likely reflects the experimental settings and stimulation strength [24]. Nevertheless, in line with our results, inhibition of NFAT by low-dose CsA increased the number of tTreg in atopic dermatitis patients [47]. It seems reasonable to establish an inverse association between SOCE signal and Treg stability. In our analysis of the RNA-seq and

350 chromatin accessibility data, we did not identify any particular mechanism that may account for the
351 distinct Ca^{2+} signal patterns in tTregs and iTregs. However, in contrast to Tconvs and iTregs, there
352 must be a negative signal loop that blunts SOCE vibration in tTregs. We tried to sustain the calcium
353 signaling in tTregs forcibly by thapsigargin, and indeed observed loss of Foxp3. However, as we at
354 the moment cannot appreciate the finesse of this regulation, the underlying molecular details will
355 require much more delicate approaches rather the brutal force of ER store depletion. In our view,
356 future investigation in this direction may lead to better understanding of Treg biology as well as
357 innovations in clinical Treg cell therapy.
358 Our results are consistent with the understanding that Treg-specific hypomethylation is crucial for
359 tTregs to stably express their Treg-specific genes [19,20]. Those epigenetic changes are mostly absent in
360 iTregs, resulting in their instability. The differences of accessibility in Treg genes were also observed
361 in our ATAC-seq data. Therefore, current treatments such as Vitamin C and CD28 blockage applied
362 to achieve demethylation and accessibility of Treg genes in iTregs are worthy attempts [44,45].
363 However, our work indicates that at least in ATAC-seq analyses, there are a cluster of activation and
364 differentiation-related peaks present in iTregs that remain silent in tTregs upon TCR stimulation.
365 Critically, these peaks were targeted by abundant NFAT in the iTreg nuclei following activation,
366 leading to the upregulation of Th genes. This tendency of deviation away from Tregs may be another
367 key player to iTreg instability. Our effort to produce highly stable iTregs would likely require a
368 combined approach to demethylate Treg-specific genes and at the same time to block the activation
369 and differentiation-related genes. In our work, targeting NFAT signaling during the restimulation
370 phase appeared to be a potential method. Other ways that can directly close these genes will also
371 likely be beneficial.
372 In this work, we stress the importance of NFAT signal in the instability of iTregs. Previous research
373 has also unveiled the adverse effects of other TCR signaling pathways on Treg stability, such as
374 NF-κB and mTOR. As all those factors may contribute to the shift in phenotype, it is out of scope of
375 this report to directly compare all those factors. However, the value of this report is the identification
376 of a key difference in Ca^{2+} signaling under TCR ligation that may explain the stability differences
377 between iTregs and tTregs, which may open the door for additional regulations given the key role of
378 SOCE activity in T cell activation.
379

380 **Methods**

381 Mice

382 All mice were in CD45.2 C57BL/6 background unless noted otherwise. OT-II-transgenic mice and
383 CD45.1 mice were purchased from Jackson Laboratories. FoxP3-IRES-GFP transgenic mice
384 (B6.Cg-Foxp3^{tm2Tch}/J, Strain #:006772 from Jackson Laboratory) were a gift from Dr. Hai Qi, School
385 of Medicine, Tsinghua University. Foxp3-RFP mice were a gift from Dr. Xuyu Zhou, Institute of
386 Microbiology, Chinese Academy of Sciences (CAS). Wild Type mice were purchased from Beijing
387 Vital River Laboratory Animal Technology Co., Ltd. All mice were bred and housed at Tsinghua
388 University Animal Facilities and maintained under specific pathogen-free conditions. All animal
389 experiments were conducted in accordance of governmental and institutional guidelines for animal
390 welfare and approved by the IACUC at the Tsinghua University.

391

392 Antibodies and Reagents

393 Recombinant Human IL-2 and human TGF-β were from R&D systems. Anti-mouse CD3 and
394 biotin-anti-CD3 (145-2C11) mAb, anti-mouse CD28 and biotin-anti-CD28 (37.51) mAb, Purified
395 Streptavidin were all from biolegend. LIVE/DEAD Fixable Aqua were from Invitrogen. For flow
396 cytometric analysis, in addition to CD45.1 (A20) monoclonal antibody from Invitrogen, others were
397 purchased from eBioscience or BD Pharmingen. The following clones were used: FoxP3(150D/E4),
398 CD45.2 (104), CD4 (GK1.5), CD25 (PC61.5), CD44 (IM7), CD62L (MEL-14). Antibody used in
399 immunoblot including NFATc1 Antibody (7A6) and NFATc2 Antibody (4G6-G5) were from Santa
400 Cruz, Lamin A/C (4C11), β-Actin (13E5) and GAPDH (D4C6R) mAb were from CST. Monoclonal
401 ANTI-FLAG® M2 antibody used in Cut&Tag assay was from Sigma. Mouse CD4 T Cell Isolation Kit
402 used for the enrichment of CD4^{+} T cells was from Stem cell. Foxp3/Transcription Factor Staining
403 Buffer Set for Foxp3 staining was from eBioscience. NE-PER^{TM} Nuclear and Cytoplasmic Extraction
404 Reagents used for immunoblot was from Thermo. All sequencing kit, including TruePrep DNA
405 Library Prep Kit V2, Hyperactive Universal CUT&Tag Assay Kit and TruePrep Index Kit V2 was
406 from Vazyme. For calcium mobilization, Ionomycin was from Beyotime and thapsigargin from
407 Invitrogen. For inhibitors, cyclosporin A, CM-4620 and BTP2 were all from MCE. $OVA_{323-339}$
408 peptides from MBL. For Calcium imaging, Fluo-4 AM was from Thermo and Indo-1 AM from BD.

409

410 Flow Cytometry sorting and FACS

411 For surface marker detection, cells were incubated with Fc blocker (CD16/32 antibody; 2.4G2) for 5
412 min, and then incubated with surface antibody for 15 min at room temperature avoiding light. Foxp3
413 intracellular staining was performed by cell fixation and permeabilization using the Foxp3/

Transcription Factor Staining Buffer Set. Samples were analyzed on Fortessa cytometers (BD) with FACS Diva software and data were analyzed with Flowjo.

To prepare Tconv, tTreg and iTreg for experiments, spleen was isolated from 2-4-month-old Foxp3-GFP mice for Tconv and tTreg sorting, and 6-week-old mice for iTreg induction. Subsequently, CD4+ T cells were enriched using CD4 Isolation kit and stained with indicated surface markers. FACSAriaII (BD) was used for collecting particular population. The cell populations used are as follows: naive T cells, $CD4^+$ Foxp3-GFP^+ $CD44^{low}$ $CD62L^{high}$; tTreg cells, $CD4^+$ Foxp3-GFP^+; iTreg, Foxp3-RFP^+ or Foxp3-GFP^+. Infected iTreg, Foxp3-RFP^+ MSCV-GFP^+.

In vitro iTreg induction and Restimulation

$CD4^+$Foxp3-GFP^- $CD62L^{hi}CD44^{lo}$ (or Foxp3-RFP^-) naive T cells were sorted using 6-week-old mice and stimulated with plate-bound 0.5 μg/mL anti-CD3 and 1 μg/mL anti-CD28 in the presence of 2 ng/mL human TGF-β and 200 U/mL rhIL-2. iTreg was induced for 4d and sorted using Foxp3-GFP/RFP fluorescence, then cells were rested in fresh RPMI complete medium containing 200 U/mL rhIL2 for 1d.

For iTreg restimulation, iTreg was harvested plated at 0.4×10^6 cells for restimulation with plate-bound 0.5 μg/mL anti-CD3 and 1 μg/mL anti-CD28 in 96 plate. After 2d restimulation, Foxp3 was analyzed by intracellular staining.

Calcium Measurment

For Calcium influx within 10min upon TCR activation, sorted Foxp3-RFP^- Tconv, Foxp3-RFP^+ tTreg and Foxp3-GFP^+ iTreg were resting for 1d, then mixed and loaded with 1 μM Indo-1 AM at 37°C for 30 min in RPMI medium without FBS. Cells were then washed for twice in cold RPMI medium containing 1% FBS, followed by staining with biotinylated anti-CD3 and biotinylated anti-CD28 on ice for 1h. For calcium measurement, cells were heated in 37°C water bath for 5 min, then the baseline was recorded for 60 s on LSR II(BD). Calcium influx was triggered by the addition of 100μg/mL streptavidin to crosslink TCR. Data were analyzed using kenetics in FlowJo.

For calcium oscillation within 1h, Foxp3-RFP^- Tconv, Foxp3-RFP^+ tTreg, and Foxp3-RFP^+ iTreg were sorted and rested for 1d, then cells were loaded with Fluo-4 AM at 37°C for 30 min. After washing twice with PBS and further incubating in RPMI medium for 10min, cells were activated by plate-bound 0.5 μg/mL anti-CD3 and 1 μg/mL anti-CD28 in poly-L-lysine-coated confocal dish. Excess non-adherent cells were removed by flushing with buffer solution after 10 min. Fluorescence were recorded in the indicated time after stimulation as a time lapse for 20 min with an interval of 6 seconds. The mean fluorescence intensity changes over time in single cells were analyzed using

Surface in Imaris and normalized to resting fluorescence F0 (Fluo-4 F/F0), further the standard deviation of F/F0 in single cells was calculated and presented using GraphPad.

Immunoblot

iTreg, tTreg and Tconv were rested for 1d in RPMI medium containing rhIL-2 and treated with cyclosporine A (CsA) for 30 min before activated. Then these cells were stimulated by plate-bound 0.5 μg/mL anti-CD3 and 1 μg/mL anti-CD28 for indicated time, in the absence or presence of TGF-β. After stimulation, cells were immediately lysed using CERI, then nuclear and cytoplasmic component were separated using NE-PER™ Nuclear and Cytoplasmic Extraction Reagents. After being mixed with SDS loading buffer and boiled for 10 min, the cytoplasmic and nuclear proteins equal to 5x10^5 iTreg and $2x10^{6}$ tTreg/Tconv were loaded onto 7.5% PAGE Gels. Then the protein was transferred onto a NC membrane and immunoblotted with NFATc1 and NFATc2, Actin and GAPDH were used as loading control of cytoplasmic protein, and LaminA/C as nuclear. Finally, the immunostained bands were detected by Super ECL Detection Reagent.

Treg cell suppression assay *in vitro*

10^4 purified DCs from splenocytes were pulsed with 2 μg/ml $OVA_{323-339}$ peptide, then iTreg and tTreg (2×10^4) were added onto DCs to occupy the latter for 30 min. $CD25^-$ OTII Tconv cells were sorted and stained by CFSE (Thermo Fisher Scientifc). 2×10^4 OTII Tconv cells were mixed in DC-Treg culture in a 96-well U bottom plate. The proliferation of OTII T cells was assessed after 2-4 d by CFSE dilution on flow cytometry.

DN-ORAI and NFAT-flag construction and Retrovirus infection

For DN-ORAI, ORAI CDS sequences were amplified from cDNA library and mutated with primer. Then WT-ORAI and DN-ORAI were linked with MSCV-GFP vector. For NFAT-Flag, Nfatc1-flag CDS was amplified from TetO-FUW-flag-Nfatc1 plasmid, and further linked with MSCV-GFP vector. For retrovirus production, platE cells were cultured with DMEM medium containing 10% FBS to 80%-90% confluence. For each 10cm dish, 10ug MSCV plasmid and 10ul Neofect transfection reagent were mixed in 500ul Opti-MEM medium. After 30 min incubation, the DNA mixture were added into the well and gently mixed. After 48 and 72 h, supernatant containing viruses was collected, filtered with 0.45um membrane. 8ug/mL polybrene was added to virus supernatant, then Foxp3-RFP+ iTreg was infected on the day 2 and 3 of induction by centrifugation at 1500g, 37°C 2h. On the day 5 of induction, the infected cells with GFP fluorescence and Foxp3-RFP iTreg was sorted and used.

482 *In vivo* iTreg stability

483 CD45.2^{+} Foxp3-RFP^{+} iTreg was sorted, and washed twice. 5X10$^{\wedge 6}$ cells were adoptively transferred
484 into CD45.1 mice via tail vein. For DN-ORAI iTreg, CD45.2^{+} Foxp3-RFP^{+} iTreg was infected and
485 GFP^{+}RFP^{+} iTreg was sorted to transfer to CD45.1 recipient. Six hours after cell transfer, mice were
486 immunized with OVA protein mixed with Alum adjuvant in each hind flank. After 4 days of
487 immunization, mLN were collected and the percentage of Foxp3+ cells in CD45.2^{+} was analyzed by
488 intracellular staining.

489

490 AFM Based Single Cell Force Spectroscopy

491 The experiments were performed as previously described using a JPK CellHesion unit[25,48]. In brief, to
492 measure Treg-DC adhesion forces in bicellular system, DC2.4 cells were cultured on untreated glass
493 disks. iTreg/tTreg/Tconv cells were sorted and rested with rhIL2 overnight. The disks were moved into
494 an AFM-compatible chamber and mounted on to the machine stage. The incubator chamber in which
495 the machine was housed was conditioned at 37°C and at 5% CO2. A clean cantilever was coated with
496 CellTak (BD), and then used to glue individual iTreg/tTreg/Tconv cells added to the disk. Only round
497 and robust cells were selected for AFM gluing. The AFM cantilever carrying a single
498 iTreg/tTreg/Tconv cell was lowered to allow T cell contact with an individual DC and to interact for 15
499 s before being moved upwards, until two cells were separated completely. The force curves were
500 acquired. The process was then repeated. For each SCFS experiment, a pair of T–DC was used to
501 generate force readings from each up and down cycle over a period of several minutes, a minimum of
502 14 force curves were collected in each T-DC pair. In all experiments, at least three such pairs were used
503 for each condition. The force curves were further processed using the JPK image processing software.

504

505 RNA-seq

506 The RNA-seq library preparation was performed by a modified SMART-seq2 protocol[49,51]. Briefly,
507 RNA was added into 4 µl elution mix made of 1 µl RT primer (10 µM), 1 µl dNTP mix (10 mM each),
508 1 µl RNase inhibitor (4 U/µl), and 1 µl H2O. Eluted samples were incubated at 72 °C for 3 min and
509 immediately placed on ice. Each sample was added with 7 µl reverse transcription (RT) mix made of
510 0.75 µl H2O, 0.1 µl Maxima RNase-minus RT (Thermo Fisher Scientific, #EP0741), 2 µl 5x Maxima
511 RT buffer, 2 µl Betaine (5 M, Sigma-Aldrich, B0300), 0.9 µl MgCl2 (100 mM), 1 µl TSO primer (10
512 µM), 0.25 µl RNase inhibitor (40 U/µl).The RT reaction was incubated at 42 °C for 90 min and
513 followed by 10 cycles of (50 °C for 2 min, 42 °C for 2 min), then heat inactivated at 70 °C for 15 min.
514 Samples were then amplified with an addition of 14 µl PCR mix made of 1 µl H2O, 0.5 µl ISPCR
515 primer (10 µM), 12.5 µl KAPA HiFi HotStart ReadyMix (KAPA Biosystems, KK2602). The PCR

516 reaction was performed as follows: 98 °C for 3 min, 22 cycles of (98 °C for 15 sec, 67 °C for 20 sec,
517 72 °C for 6 min), and final extension at 72 °C for 5 min.
518 The amplified cDNA product was purified using VAHTS DNA Clean Beads. Sequencing libraries
519 were prepared using TruePrep DNA Library Prep Kit V2 for Illumina (Vazyme, TD503-02).
520 Primer sequences: RT primer (Sangon), 5'Biotin-AAGCAGTGGTATCAACGCAGAGTACTTTTTT
521 TTTTTTTTTTTTTTTTTTTTTTTTVN; TSO primer (Sangon), 5'Biotin-AAGCAGTGGTATCAAC
522 CAGAGTACAT/rG//rG//iXNA_G/; ISPCR primer (Sangon), 5'Biotin-AAGCAGTGGTATCAACGC
523 AGA*G*T.
524
525 RNA-seq analysis
526 Raw fastq reads were trimmed by Cutadapt (version 1.18) to trim adapter and low quality sequence.
527 Reads were aligned to the mouse genome (mm10) using STAR (version 2.5.3). The number of reads
528 within each gene in each single cell were counted using RSEM (version 1.3.0) with gene annotation
529 file from GENCODE (GRCm38.m23).
530 Differential expression was estimated by using DESeq2 package (version 1.26) with absolute log2
531 Fold change > 0.5 and adjusted P value < 0.05.
532 Functional enrichment analysis were performed by using the clusterProfiler R package (v3.14.3) with
533 default parameters (P value < 0.05) and the functional annotations terms in Gene Ontology (GO)[50].
534
535 ATAC-sequencing
536 ATAC-seq were performed using TruePrep DNA Library Prep Kit V2 for Illumina according to the
537 manufacturer's recommendation. Briefly, live cells were sorted using PI staining, then 5×10^4 cells
538 were transferred to a low-binding centrifuge tube and resuspended in 50 μL of pre-chilled Lysis Buffer.
539 After 20 times pipetting, cells were incubated on ice for 10 minutes for lysis. Subsequently, cells were
540 pelleted by centrifugation at 4°C 500 g for 5 minutes, and suspended in a mixture consisting of 10 μL
541 of 5× TTBL, 5 μL of TTE Mix V50, and 35 μL of ddH2O. The mixture was gently mixed by pipetting
542 20 times, and incubated at 37°C for 30 minutes for fragmentation. The products were purified using 2×
543 VAHTS DNA Clean Beads, eluted with 26 μL of water, and collected for the subsequent amplification.
544 24 μl of the eluted samples were amplified with different combination of i7 index and i5 index primers.
545 QPCR were performed to determine the cycle number for PCR amplification. 0.55×VAHTS DNA
546 Clean Beads was employed for size selection of the PCR product. Finally, 30 ng of each sample were
547 pooled for subsequent second-generation sequencing, on the Illumina NovaSeq 6000 with read length
548 of 150 bp.
549

550 ATAC-seq analysis
551 Raw fastq reads were trimmed by Cutadapt (version 1.18) to trim adapter and low quality sequence.
552 Reads were aligned to the mouse genome (mm10) using Bowtie2 (version 2.3.3.1), the parameters are
553 -t -q -N 1 -L 25 -X 2000 --no-mixed --no-discordant.
554 Reads with alignment quality < Q30, mapped to chrM, overlapping with ENCODE blacklisted regions)
555 were discarded. Duplicates were removed using Picard (version 2.20.4) and Samtools (version 1.13).
556 Open chromatin region peaks were called on using MACS2 peak caller (version 2.2.7.1) with the
557 following parameters: -nomodel -nolambda -call-summits. Peaks from all samples were merged and
558 peaks falls in ENCODE blacklisted regions were filtered out.
559 Differential peaks were estimated by using "edgeR" method in the R package DiffBind (version 2.14.0)
560 with absolute log2 Fold change > 1 and adjusted P value < 0.05.
561 The peaks annotations were performed with the "annotatePeak" function in the R package
562 ChIPseeker[52].
563 The plot of ATAC-seq signals over a set of genomic regions were calculated by using "computeMatrix"
564 function in deepTools (version 2.0) and plotted by using "plotHeatmap" and "plotProfile" functions in
565 deepTools.
566
567
568 Cut&Tag assay
569 Foxp3-RFP+ iTreg were induced, and infected with NFAT-Flag-GFP lentiviruses on day 1.5 and day
570 2.5 of induction. On day 5, Foxp3-RFP+ MSCV-NFAT-Flag-GFP+ iTregs were sorted, then rested and
571 restimulated for 2 day. Cut&Tag assay were performed using Hyperactive Universal CUT&Tag Assay
572 Kit for Illumina (Vazyme Biotech Co.,Ltd) according to the manufacturer's recommendation. Briefly,
573 1×10^5 iTregs were collected to low-binding centrifuge tubes and washed. Nucleus isolation were
574 performed by NE buffer for 10 min on ice, and cross-linked by 0.1% formaldehyde for 2 min, then
575 stopped by glycine. Con A Beads were pre-treated with binding buffer, and then incubated with nuclei
576 of iTreg for 10 min. Further, samples were incubated with anti-Flag M2 antibody (1:50) or without
577 primary antibody (Mock) overnight at 4°C. Goat Anti-Mouse IgG secondary antibody (1:50) was
578 added and incubated for 1 h. Cells were washed three times, and then incubated with pA/G-Tnp
579 enzyme for 1 h. After incubation, samples were mixed with 5×TTBL and Dig-300 Buffer and
580 incubated at 37°C for 60 min for fragmentation. DNA was extracted and purified, then amplified with
581 different combination of i7 index and i5 index primers. QPCR was performed to determine the cycle
582 number for PCR amplification. VAHTS DNA Clean Beads were employed for size selection of the
583 PCR product. Finally, 30 ng of each sample were pooled for subsequent second-generation sequencing,

584 on the Illumina NovaSeq 6000 with read length of 150 bp.
585
586 Cut&Tag data analysis
587 Raw fastq reads were trimmed by Cutadapt (version 1.18) to trim adapter and low quality sequence.
588 Reads were aligned to the mouse genome (mm10) using Bowtie2 (version 2.3.3.1), the parameters are
589 -t -q -N 1 -L 25 -X 2000 --no-mixed --no-discordant.
590 Reads with alignment quality < Q30, mapped to chrM, overlapping with ENCODE blacklisted regions
591 (https://sites.google.com/site/anshulkundaje/projects/blacklists) were discarded. Duplicates were
592 removed using Picard (version 2.20.4) and Samtools (version 1.13). Open chromatin region peaks
593 were called using MACS2 peak caller (version 2.2.7.1) with the following parameters: -nomodel
594 -nolambda -call-summits. Peaks from all samples were merged and peaks falls in ENCODE
595 blacklisted regions were filtered out.
596 The peaks annotations were performed with the "annotatePeak" function in the R package
597 ChIPseeker[52].
598 The plot of Cut&Tag signals over a set of genomic regions were calculated by using "computeMatrix"
599 function in deepTools and plotted by using "plotHeatmap" and "plotProfile" functions in deepTools.
600 The motif enrichment analysis was performed by using the "findMotifsGenome.pl" command in
601 HOMER with default parameters.
602 The motif occurrences in each peak were identified by using FIMO (MEME suite v5.0.4) with the
603 following settings: a first-order Markov background model, a P value cutoff of 10^{-4}, and PWMs from
604 the mouse HOCOMOCO motif database (v11).
605
606 Statistical analysis
607 Calculation and graphing were done with Prism (GraphPad). Data were presented as mean ± SEM,
608 unless indicated otherwise. Student's t test was used for comparing endpoint means of different groups.
609 P value < 0.05 was considered significant. *, P < 0.05; **, < 0.01; ***, < 0.001; ****, < 0.0001; N.S.,
610 not significant. Numbers of independently-performed experiment repeats are shown as N, biological
611 replicates of each experiment as n.
612
613
614

Acknowledgments

We thank Dr. Hai Qi for providing Foxp3-GFP mice, platE cell line and guidance of calcium-related experimental design. We thank Dr. Saiyong Zhu for providing TetO-FUW-flag-Nfatc1 plasmid. We also thank Imaging Core Facility, Technology Center for Protein Sciences of Tsinghua University for assistance. Y.S. is supported by the joint Peking-Tsinghua Center for Life Sciences, the National Natural Science Foundation of China General Program (31370878), State Key Program (31630023) and Innovative Research Group Program (81621002), by grants from CIHR (PJT-156334 and PJT-166155) and NSERC (RGPIN/03748-2018).

Author Contributions

H.L. performed all the experiments unless noted otherwise. G.Y. and H.L. perform RNA-seq experiment and all sequencing data analysis. X.L. performed AFM-related experiments. X.W. and S.G. provides suggestions to calcium-related expreiments and RNA-seq data analysis. T.X. provided biophysical mechanism on cell adhesion. X.Z. provided critical review on Treg biology. Y.L. provided critical technical support for sequencing experiment and data analysis. X.H. provided overall critical insight. Y.S. was responsible for the overall design and wrote the manuscript with inputs from X.H.

Reference

1. Rudensky, A.Y. (2011). Regulatory T cells and Foxp3. Immunological Reviews *241*, 260–268. 10.1111/j.1600-065X.2011.01018.x.
2. Sakaguchi, S., Yamaguchi, T., Nomura, T., and Ono, M. (2008). Regulatory T Cells and Immune Tolerance. Cell *133*, 775–787. 10.1016/j.cell.2008.05.009.
3. Fontenot, J.D., Dooley, J.L., Farr, A.G., and Rudensky, A.Y. (2005). Developmental regulation of Foxp3 expression during ontogeny. Journal of Experimental Medicine *202*, 901–906. 10.1084/jem.20050784.
4. Curotto de Lafaille, M.A., Lino, A.C., Kutchukhidze, N., and Lafaille, J.J. (2004). CD25− T Cells Generate CD25+Foxp3+ Regulatory T Cells by Peripheral Expansion. The Journal of Immunology *173*, 7259–7268. 10.4049/jimmunol.173.12.7259.
5. Apostolou, I., and von Boehmer, H. (2004). In Vivo Instruction of Suppressor Commitment in Naive T Cells. Journal of Experimental Medicine *199*, 1401–1408. 10.1084/jem.20040249.
6. Cobbold, S.P., Castejon, R., Adams, E., Zelenika, D., Graca, L., Humm, S., and Waldmann, H. (2004). Induction of *foxP3* + Regulatory T Cells in the Periphery of T Cell Receptor Transgenic Mice Tolerized to Transplants. The Journal of Immunology *172*, 6003–6010. 10.4049/jimmunol.172.10.6003.
7. Chen, W., Jin, W., Hardegen, N., Lei, K., Li, L., Marinos, N., McGrady, G., and Wahl, S.M. (2003). Conversion of Peripheral CD4+CD25- Naive T Cells to CD4+CD25+ Regulatory T Cells by TGF-beta Induction of Transcription Factor Foxp3. Journal of Experimental Medicine *198*, 1875-1886. 10.1084/jem.20030152.
8. Fantini, M.C., Becker, C., Monteleone, G., Pallone, F., Galle, P.R., and Neurath, M.F. (2004). Cutting Edge: TGF-β Induces a Regulatory Phenotype in CD4+CD25− T Cells through Foxp3 Induction and Down-Regulation of Smad7. The Journal of Immunology *172*, 5149–5153. 10.4049/jimmunol.172.9.5149.
9. Shevach, E.M., and Thornton, A.M. (2014). tTregs, pTregs, and iTregs: similarities and differences. Immunol Rev *259*, 88–102. 10.1111/imr.12160.
10. Fu, S., Zhang, N., Yopp, A.C., Chen, D., Mao, M., Chen, D., Zhang, H., Ding, Y., and Bromberg, J.S. (2004). TGF-beta Induces Foxp3 + T-Regulatory Cells from CD4 + CD25 - Precursors. Am J Transplant *4*, 1614–1627. 10.1111/j.1600-6143.2004.00566.x.
11. Singh, A.K., Horvath, K.A., and Mohiuddin, M.M. (2009). Rapamycin Promotes the Enrichment of CD4+CD25hiFoxP3+ T Regulatory Cells From Naïve CD4+ T Cells of Baboon That Suppress Antiporcine Xenogenic Response In Vitro. Transplantation Proceedings *41*, 418–421. 10.1016/j.transproceed.2008.10.079.

12. Rubtsov, Y.P., Niec, R.E., Josefowicz, S., Li, L., Darce, J., Mathis, D., Benoist, C., and Rudensky, A.Y. (2010). Stability of the Regulatory T Cell Lineage in Vivo. Science *329*, 1667–1671. 10.1126/science.1191996.

13. Floess, S., Freyer, J., Siewert, C., Baron, U., Olek, S., Polansky, J., Schlawe, K., Chang, H.-D., Bopp, T., Schmitt, E., et al. (2007). Epigenetic Control of the foxp3 Locus in Regulatory T Cells. PLoS Biol *5*, e38. 10.1371/journal.pbio.0050038.

14. Chen, Q., Kim, Y.C., Laurence, A., Punkosdy, G.A., and Shevach, E.M. (2011). IL-2 Controls the Stability of Foxp3 Expression in TGF-β–Induced Foxp3 $^{+}$ T Cells In Vivo. J.I. *186*, 6329–6337. 10.4049/jimmunol.1100061.

15. Koenecke, C., Czeloth, N., Bubke, A., Schmitz, S., Kissenpfennig, A., Malissen, B., Huehn, J., Ganser, A., Förster, R., and Prinz, I. (2009). Alloantigen-specific *de novo*- induced Foxp3 $^{+}$ Treg revert *in vivo* and do not protect from experimental GVHD. Eur. J. Immunol. *39*, 3091–3096. 10.1002/eji.200939432.

16. Ohkura, N., Kitagawa, Y., and Sakaguchi, S. (2013). Development and Maintenance of Regulatory T cells. Immunity *38*, 414–423. 10.1016/j.immuni.2013.03.002.

17. Fu, W., Ergun, A., Lu, T., Hill, J.A., Haxhinasto, S., Fassett, M.S., Gazit, R., Adoro, S., Glimcher, L., Chan, S., et al. (2012). A multiply redundant genetic switch "locks in" the transcriptional signature of regulatory T cells. Nat Immunol *13*, 972–980. 10.1038/ni.2420.

18. Hill, J.A., Feuerer, M., Tash, K., Haxhinasto, S., Perez, J., Melamed, R., Mathis, D., and Benoist, C. (2007). Foxp3 Transcription-Factor-Dependent and -Independent Regulation of the Regulatory T Cell Transcriptional Signature. Immunity *27*, 786–800. 10.1016/j.immuni.2007.09.010.

19. Samstein, R.M., Arvey, A., Josefowicz, S.Z., Peng, X., Reynolds, A., Sandstrom, R., Neph, S., Sabo, P., Kim, J.M., Liao, W., et al. (2012). Foxp3 Exploits a Pre-Existent Enhancer Landscape for Regulatory T Cell Lineage Specification. Cell *151*, 153–166. 10.1016/j.cell.2012.06.053.

20. Ohkura, N., Hamaguchi, M., Morikawa, H., Sugimura, K., Tanaka, A., Ito, Y., Osaki, M., Tanaka, Y., Yamashita, R., Nakano, N., et al. (2012). T Cell Receptor Stimulation-Induced Epigenetic Changes and Foxp3 Expression Are Independent and Complementary Events Required for Treg Cell Development. Immunity *37*, 785–799. 10.1016/j.immuni.2012.09.010.

21. van der Veeken, J., Gonzalez, A.J., Cho, H., Arvey, A., Hemmers, S., Leslie, C.S., and Rudensky, A.Y. (2016). Memory of Inflammation in Regulatory T Cells. Cell *166*, 977–990. 10.1016/j.cell.2016.07.006.

22. Sumpter, T.L., Payne, K.K., and Wilkes, D.S. (2008). Regulation of the NFAT pathway discriminates CD4+CD25+ regulatory T cells from CD4+CD25– helper T cells. J Leukoc Biol *83*, 708-717. 10.1189/jlb.0507321

710 23. Vaeth, M., Schliesser, U., Muller, G., Reissig, S., Satoh, K., Tuettenberg, A., Jonuleit, H.,
711 Waisman, A., Muller, M.R., Serfling, E., et al. (2012). Dependence on nuclear factor of activated
712 T-cells (NFAT) levels discriminates conventional T cells from Foxp3+ regulatory T cells. Proceedings
713 of the National Academy of Sciences *109*, 16258–16263. 10.1073/pnas.1203870109.
714 24. Yan, D., Farache, J., Mingueneau, M., Mathis, D., and Benoist, C. (2015). Imbalanced signal
715 transduction in regulatory T cells expressing the transcription factor FoxP3. Proc Natl Acad Sci U S A
716 *112*, 14942-14947. 10.1073/pnas.1520393112
717 25. Chen, J., Ganguly, A., Mucsi, A.D., Meng, J., Yan, J., Detampel, P., Munro, F., Zhang, Z., Wu, M.,
718 Hari, A., et al. (2017). Strong adhesion by regulatory T cells induces dendritic cell cytoskeletal
719 polarization and contact-dependent lethargy. The Journal of Experimental Medicine *214*, 327–338.
720 10.1084/jem.20160620.
721 26. Wang, X., Geng, S., Meng, J., Kang, N., Liu, X., Xu, Y., Lv, H., Xu, Y., Xu, X., Song, X., et al.
722 (2022). FoxP3-mediated blockage of ryanodine receptor 2 is the molecular basis for the contact-based
723 suppression by regulatory T cells. BioRxiv. 10.1101/2022.05.02.490213.
724 27. Selvaraj, R.K., and Geiger, T.L. (2007). A Kinetic and Dynamic Analysis of Foxp3 Induced in T
725 Cells by TGF-β. J Immunol *178*, 7667–7677. 10.4049/jimmunol.178.12.7667.
726 28. Guse, A.H. (1998). Ca2+ signaling in T-Lymphocytes. Crit.Rev.Immuno *18*, 419–448.
727 10.1615/CritRevImmunol.v18.i5.20
728 29. Christo, S.N., Diener, K.R., and Hayball, J.D. (2015). The functional contribution of calcium ion
729 flux heterogeneity in T cells. Immunol Cell Biol *93*, 694–704. 10.1038/icb.2015.34.
730 30. Wülfing, C., Rabinowitz, J.D., Beeson, C., Sjaastad, M.D., McConnell, H.M., and Davis, M.M.
731 (1997). Kinetics and Extent of T Cell Activation as Measured with the Calcium Signal. Journal of
732 Experimental Medicine *185*, 1815–1825. 10.1084/jem.185.10.1815.
733 31. Dolmetsch, R.E., Xu, K., and Lewis, R.S. (1998). Calcium oscillations increase the efficiency and
734 specificity of gene expression. Nature *392*, 933-936. 10.1038/31960.
735 32. Le Borgne, M., Raju, S., Zinselmeyer, B.H., Le, V.T., Li, J., Wang, Y., Miller, M.J., and Shaw,
736 A.S. (2016). Real-Time Analysis of Calcium Signals during the Early Phase of T Cell Activation
737 Using a Genetically Encoded Calcium Biosensor. J.I. *196*, 1471–1479. 10.4049/jimmunol.1502414.
738 33. Dolmetsch, R.E., Lewis, R.S., and Goodnowt, C.C. (1997). Differential activation of transcription
739 factors induced by Ca2 + response amplitude and duration. Nature *386*, 855–858. 10.1038/386855a0
740 34. Tomida, T. (2003). NFAT functions as a working memory of Ca2+ signals in decoding Ca2+
741 oscillation. The EMBO Journal *22*, 3825–3832. 10.1093/emboj/cdg381.
742 35. Serfling, E., Chuvpilo, S., Liu, J., Höfer, T., and Palmetshofer, A. (2006). NFATc1 autoregulation:
743 a crucial step for cell-fate determination. Trends in Immunology *27*, 461–469.

744 10.1016/j.it.2006.08.005.
745 36. Zhou, B., Cron, R.Q., Wu, B., Genin, A., Wang, Z., Liu, S., Robson, P., and Baldwin, H.S. (2002).
746 Regulation of the Murine Nfatc1 Gene by NFATc2. Journal of Biological Chemistry *277*, 10704–
747 10711. 10.1074/jbc.M107068200.
748 37. Nayak, A., Glöckner-Pagel, J., Vaeth, M., Schumann, J.E., Buttmann, M., Bopp, T., Schmitt, E.,
749 Serfling, E., and Berberich-Siebelt, F. (2009). Sumoylation of the Transcription Factor NFATc1 Leads
750 to Its Subnuclear Relocalization and Interleukin-2 Repression by Histone Deacetylase. J. Biol. Chem.
751 *284*, 10935–10946. 10.1074/jbc.M900465200.
752 38. Li, X., Liang, Y., LeBlanc, M., Benner, C., and Zheng, Y. (2014). Function of a Foxp3 cis
753 -Element in Protecting Regulatory T Cell Identity. Cell *158*, 734–748. 10.1016/j.cell.2014.07.030.
754 39. Zheng, Y., Josefowicz, S., Chaudhry, A., Peng, X.P., Forbush, K., and Rudensky, A.Y. (2010).
755 Role of conserved non-coding DNA elements in the Foxp3 gene in regulatory T-cell fate. Nature *463*,
756 808–812. 10.1038/nature08750.
757 40. Tone, Y., Furuuchi, K., Kojima, Y., Tykocinski, M.L., Greene, M.I., and Tone, M. (2008). Smad3
758 and NFAT cooperate to induce Foxp3 expression through its enhancer. Nat Immunol *9*, 194–202.
759 10.1038/ni1549.
760 41. Mignen, O., Thompson, J.L., and Shuttleworth, T.J. (2008). Orai1 subunit stoichiometry of the
761 mammalian CRAC channel pore: CRAC channel subunit stoichiometry. The Journal of Physiology
762 *586*, 419–425. 10.1113/jphysiol.2007.147249.
763 42. Akamatsu, M., Mikami, N., Ohkura, N., Kawakami, R., Kitagawa, Y., Sugimoto, A., Hirota, K.,
764 Nakamura, N., Ujihara, S., Kurosaki, T., et al. (2019). Conversion of antigen-specific effector/memory
765 T cells into Foxp3-expressing T_{reg} cells by inhibition of CDK8/19. Sci. Immunol. *4*, eaaw2707.
766 10.1126/sciimmunol.aaw2707.
767 43. Hill, J.A., Hall, J.A., Sun, C.-M., Cai, Q., Ghyselinck, N., Chambon, P., Belkaid, Y., Mathis, D.,
768 and Benoist, C. (2008). Retinoic Acid Enhances Foxp3 Induction Indirectly by Relieving Inhibition
769 from CD4+CD44hi Cells. Immunity *29*, 758–770. 10.1016/j.immuni.2008.09.018.
770 44. Mikami, N., Kawakami, R., Chen, K.Y., Sugimoto, A., Ohkura, N., and Sakaguchi, S. (2020).
771 Epigenetic conversion of conventional T cells into regulatory T cells by CD28 signal deprivation. Proc
772 Natl Acad Sci USA *117*, 12258–12268. 10.1073/pnas.1922600117.
773 45. Yue, X., Trifari, S., Äijö, T., Tsagaratou, A., Pastor, W.A., Zepeda-Martínez, J.A., Lio, C.-W.J.,
774 Li, X., Huang, Y., Vijayanand, P., et al. (2016). Control of Foxp3 stability through modulation of TET
775 activity. Journal of Experimental Medicine *213*, 377–397. 10.1084/jem.20151438.
776 46. Zhang, P., Tey, S.-K., Koyama, M., Kuns, R.D., Olver, S.D., Lineburg, K.E., Lor, M., Teal, B.E.,
777 Raffelt, N.C., Raju, J., et al. (2013). Induced Regulatory T Cells Promote Tolerance When Stabilized

778 by Rapamycin and IL-2 In Vivo. J.I. *191*, 5291–5303. 10.4049/jimmunol.1301181.
779 47. Brandt, C., Pavlovic, V., Radbruch, A., Worm, M., and Baumgrass, R. (2009). Low-dose
780 cyclosporine A therapy increases the regulatory T cell population in patients with atopic dermatitis.
781 Allergy *64*, 1588–1596. 10.1111/j.1398-9995.2009.02054.x.
782 48. Flach, T.L., Ng, G., Hari, A., Desrosiers, M.D., Zhang, P., Ward, S.M., Seamone, M.E., Vilaysane,
783 A., Mucsi, A.D., Fong, Y., et al. (2011). Alum interaction with dendritic cell membrane lipids is
784 essential for its adjuvanticity. Nat Med *17*, 479–487. 10.1038/nm.2306.
785 49. Habib, N., Li, Y., Heidenreich, M., Swiech, L., Avraham-Davidi, I., Trombetta, J.J., Hession, C.,
786 Zhang, F., and Regev, A. (2016). Div-Seq: Single-nucleus RNA-Seq reveals dynamics of rare adult
787 newborn neurons. Science *353*, 925–928. 10.1126/science.aad7038.
788 50. Ashburner, M., Ball, C.A., Blake, J.A., Botstein, D., Butler, H., Cherry, J.M., Davis, A.P.,
789 Dolinski, K., Dwight, S.S., Eppig, J.T., et al. (2000). Gene Ontology: tool for the unification of biology.
790 Nat Genet *25*, 25–29. 10.1038/75556.
791 51. Picelli, S., Faridani, O.R., Björklund, Å.K., Winberg, G., Sagasser, S., and Sandberg, R. (2014).
792 Full-length RNA-seq from single cells using Smart-seq2. Nat Protoc *9*, 171–181.
793 10.1038/nprot.2014.006.
794 52. Yu, G., Wang, L.-G., and He, Q.-Y. (2015). ChIPseeker: an R/Bioconductor package for ChIP
795 peak annotation, comparison and visualization. Bioinformatics *31*, 2382–2383.
796 10.1093/bioinformatics/btv145.
797
798
799
800
801
802
803
804
805
806
807
808
809
810
811
812

Figures

Fig 1. iTreg share similar suppressive mechanism to tTregs

A. Comparison of suppressive activity between tTreg and iTreg. CFSE-labelled OT-II T cells were stimulated with OVA-pulsed DC, then Foxp3-GFP^{+} iTregs and tTregs were added to the culture to suppress the OT-II proliferation. After 4 days, CFSE dilution were analyzed. n=3, N=3. Left, Representative histograms of CFSE in divided Tconvs. Right, graph for the percentage of divided Tconvs.

B. iTregs possessed stronger binding force to DCs than tTreg. A schematic diagram for AFM-SCFS assay setup (left). SCFS force readings for Tconv, tTreg and iTreg adhering to DC2.4 cells, one line represents a pair of T-DC, every dot represents force reading from each contact. Mean force of Tconv, tTreg and iTregs adhering to DC2.4 cells.

C. iTregs showed increased binding force compared with activated Tconvs. Mean force of Tconv, activated Tconv and iTreg adhering to DC2.4 cells. n>45, N=3.

D. Precise expression of FoxP3 was assessed during iTreg induction. Naïve Tconvs were stimulated with anti-CD3 and anti-CD28, in the presence of TGF-β and IL2 to induce iTregs. Cells were harvested at the indicated time and Foxp3 expression was analyzed by intracellular staining.

E. Basal Ca^{2+} oscillation was assessed during iTreg induction. Naïve Tconvs were stimulated with anti-CD3 and anti-CD28, in the presence of TGF-β and IL2 to induce iTregs. Cells were harvested at the indicated time and loaded with Fluo-4 AM, and Fluo-4 fluorescence over time were recorded with confocal microscope. The change of intracellular free Ca^{2+} concentration over time were shown as F/F0. The ratio of oscillated cells and standard deviation of F/F0 were calculated. n>150, N=3.

Here, **, $P < 0.01$; ***, $P < 0.001$; ****, $P < 0.0001$, by students's t test.

847 **Fig 2. Diminished SOCE signal and NFAT translocation in tTregs, but not in iTregs**

848 A. Comparison of Treg stability between tTregs and iTregs. iTregs and tTregs were sorted and
849 restimulated with anti-CD3 and anti-CD28 antibodies. Cells were harvested after 2 d restimulation
850 and Foxp3 expression was analyzed by intracellular staining. The percentages of $Foxp3^+$ cells
851 were monitored by FACS. Left, representative histograms of restimulated iTregs. Right, graph for
852 the percentage of $Foxp3^+$ cells in all $CD4^+$ cells. n=4, N=5.

853 B. Early SOCE signal was measured in iTreg, tTreg and Tconv by flow cytometry. Sorted
854 Foxp3-RFP^+ iTreg and Foxp3-GFP^+ tTreg and double negative Tconv cells were mixed and
855 loaded with Indo-1 AM, then stained with biotin-anti-CD3 and biotin anti-CD28 for 1 h, the base
856 line fluorescence was recorded for 1 min, and then TCR crosslink was perform by the addition of
857 streptavidin. Left, the gate of three mixed cells. Right, Indo-1 AM ratio of these cells upon TCR
858 crosslink. N=3.

859 C. Long term SOCE were truncated in tTreg, but sustained in iTreg. Tconv, tTreg, and iTreg cells
860 were loaded with Fluo-4 AM and activated by anti-CD3 and anti-CD28 in confocal dish.
861 Fluorescence was recorded in the indicated time after stimulation with the interval of 10 s. Left,
862 the F/F0 of mean fluorescence intensities were calculated and presented, Right, graph for standard
863 deviation of fluorescence in these cells. n>50, N=3.

864 D. NFAT accumulate much in nucleus of iTreg, but not in tTreg. Tconv, tTreg, and iTreg cells were
865 stimulated by anti-CD3 and anti-CD28, after the indicated times, cells were lysed and the
866 cytoplasmic/nuclear components were separated. The cytoplasmic and nuclear NFATc1 and
867 NFATc2 were analyzed by western blot. Actin and GAPDH were used as loading control of
868 cytoplasmic proteins, and LaminA/C as nuclear. N=4.

869 E. Forcibly sustained calcium signal destabilizes tTreg. Foxp3-RFP^+ tTregs were stimulated by
870 anti-CD3 and anti-CD28. After 1 h, various concentrations TG were added in the culture medium.
871 Cells were collected after 24 h stimulation and Foxp3 expression was analyzed by intracellular
872 staining. Left, representative histograms of treated tTregs. Right, graph for the percentage of
873 $Foxp3^+$ cells in all tTregs. n=3, N=3.

874 Here, *, $P < 0.05$; **, $P < 0.01$; ***, $P < 0.001$; ****, $P < 0.0001$, by students's t test.

875
876
877
878
879
880

881 **Fig 3. iTregs display highly open chromatin state at the activation and differentiation-related**
882 **genes**

883 A. PCA visualization of transcriptional profiles of Tconvs, tTregs and iTregs with or without TCR
884 stimulation. Color indicates cell types.
885 B. PCA visualization of chromatin accessibility profiles of different cell types. Color indicates cell
886 type.
887 C. Heatmap showing the chromatin accessibility of cell type specifically accessible peaks. As
888 shown, two major groups of genes were labelled on right.
889 D. Line plots (top) and heatmaps (bottom) of activation regions in Tconvs, iTregs and tTregs.
890 Activation regions were determined by a threshold of adjusted $P<0.05$ calculated by DESeq2.
891 E. Line plots (top) and heatmaps (bottom) of Treg regions in Tconvs, iTregs and tTregs. Treg regions
892 were determined by a threshold of adjusted $P<0.05$ calculated by DESeq2.
893 F. Genomic track showing the chromatin accessibility of Ifng, Il4, Il17ra, Il21.
894 G. Genomic track showing the chromatin accessibility of Foxp3, Ctla4.
895
896
897
898
899
900
901
902
903
904
905
906
907
908
909
910
911
912
913
914

915 **Fig 4. SOCE signaling and NFAT can disrupt iTreg stability**

916 A. Impact of calcium signal and NFAT on iTreg stability. Sorted Foxp3-GFP$^+$ iTregs were rested for
917 1d, then restimulated by anti-CD3 and CD28 in the presence of CsA and CM-4620. Percentages of
918 Foxp3$^+$ cells were analyzed by intracellular staining after 2d restimulation. Left, representative
919 histograms of CsA and CM-4620-treated iTregs. Right, graph for the percentages of CsA and
920 CM-4620-treated Foxp3$^+$ cells in all CD4$^+$ cells. n=4, N=8.

921 B. Heatmap showing the decreased changes for restimulated iTregs with CM-4620 or CsA. Typical
922 genes were highlighted.

923 C. PCA visualization of transcriptional profiles of iTregs at different states. Color indicates cell
924 states.

925 D. Venn plot showing the overlap of DEGs rescued by adding CM-4620 or CsA.

926 E. Biological terms enriched by the significant upregulated genes after iTreg restimulation rescued
927 by inhibiting Calcium or NFAT.

928 F. Representative genes upregulated after iTreg restimulation rescued by inhibiting Calcium or
929 NFAT.

930 G. QPCR of Foxp3 and Th-differentiated gene expression in the resting, restimulated and
931 CsA/CM-4620-treated iTregs.

932 Here, *, $P < 0.05$; **， $p<0.01$, by students's t test.

933

934 **Fig 5. NFAT disrupt iTreg stability by upregulating prime opened T_H genes**

935 A. Model of CUT&Tag experiments to capture the binding sites of NFATc1.

936 B. The number of NFAT Cut&Tag peaks in mock control, resting iTregs, and restimulated iTregs.

937 C. Normalized counts of ATAC-seq reads in resting and activated Tconvs, resting and activated
938 tTregs and iTregs, centered on the TSS region of NFAT-upregulated T_H genes.

939 D. Normalized counts of NFAT Cut&Tag reads in resting and restimulated iTreg, centered on the TSS
940 region NFAT-upregulated T_H genes.

941 E. Genome track visualization of NFAT binding profiles and chromatin accessibility profiles in
942 typical genes Il21, Il12rb2, and Tbx21.

943 F. Motif enriched in peaks with higher NFAT Cut&Tag signals in restimulated iTreg versus resting
944 iTreg. List of five representative motifs ranked based on the p-values. The enrichment was
945 performed by using HOMER.

946 G. The enrichment of motif occurrence for typical NFAT co-factors Smad, Fos/Jun, Rorc in the
947 NFAT peaks in NFAT-upregulated or NFAT-downregulated genes after restimulation. P-value
948 was from fisher's exact test.

949 H. IL-21 secretion in tTreg and iTreg upon activation. iTregs and tTregs were sorted and restimulated
950 with anti-CD3 and anti-CD28 antibodies, in the presence of CsA and CM-4620. Cell culture
951 supernatants were harvested after 2 d restimulation and IL-21 secretion was analyzed by ELISA.
952 n=3.

953
954
955
956
957
958
959
960
961
962
963
964
965
966
967

Fig 6. Manipulation of SOCE can enhance iTreg stability

A. Manipulation of SOCE signal by dominant negative ORAI (DN-ORAI). SOCE was recorded in DN-ORAI iTreg cells loaded with Fura-Red by flow cytometry, TG was added after 1 min to induce ER depletion, 5 mins later 2 mM calcium was added to induce calcium influx. N=3.

B. Stability of iTreg was enhanced by DN-ORAI. iTregs were infected with WT-ORAI and DN-ORAI, and then restimulated by anti-CD3 and CD28 for 2 d. Percentages of Foxp3 were analyzed by intracellular staining. Left, representative histograms of Foxp3 expression in DN-ORAI iTregs. Right, graph for the percentages of $Foxp3^+$ cells in all CD4+ cells. n=3, N=3.

C. DN-ORAI enhances iTreg suppressive capacity. CFSE-labelled OT-II T cells were stimulated with OVA-pulsed DC, Foxp3-GFP^+ WT-ORAI/DN-ORAI iTregs were added to the culture to suppress the OT-II proliferation. After 40 hours, CFSE dilutions were analyzed. n=3, N=3.

D. Stability of DN-ORAI iTreg *in vivo*. WT-ORAI/DN-ORAI-GFP^+-transfected $CD45.2^+$ Foxp3-RFP^+ OT-II iTregs were transferred i.v. into CD45.1 mice. Recipients were immunized with OVA323-339 in Alum adjuvant. On day 5, mLN and spleen were harvested and analyzed for Foxp3 expression by intracellular staining. Up, Schematic representation of adoptive transfer experiment. Bottom right, histograms of Foxp3 expression in $CD4^+CD45.1^+$cells in spleen and mLN; Bottom left, graph for the percentages of $Foxp3^+$ cells in all $CD45.2^+$ cells in mLN. n=3, N=3.

E. Proposed model. The diminished calcium signal and closed chromatin structure in tTregs protect them from genetic and epigenetic disturbances, and the sustained calcium signal in iTregs cause NFAT aggregation in the nucleus, which makes use of a pre-opened gene loci to upregulate T_H genes, thus resulting the instability of iTregs.

Here, *, $P < 0.05$; **, $P < 0.01$; ****, $P < 0.0001$, by students's t test.

1002 **Supplementary Figures**

1003 **Fig S1. Expression of Ryr2 in iTreg and the effect of Ryr2 on iTreg induction**

1004 A. QPCR for Ryr2 mRNA expression in iTregs, tTregs and Tconvs. n=3, N=4.

1005 B. The effect of Ryr2 expression on iTreg induction. Naïve Tconv cells were sorted from Ryr2 fl/fl;
1006 CD4 cre mice and control Ryr2 fl/fl mice, then cells were differentiated into iTregs for 4 d. The
1007 percentages of $Foxp3^+$ cells were analyzed by intracellular staining after 4 d induction. Left,
1008 representative histograms of induced iTregs. Right, graph for the percentage of $Foxp3^+$ cells in all
1009 $CD4^+$ cells. n=3, N=3.

1010 Here, ***, $P < 0.001$, by students's t test.

1011

1012

1013 **Fig S2. TCR responsiveness and NFAT translocation in tTregs and iTregs**

1014 A. Calcium oscillation were recorded in steady state and after anti-CD3 and anti-CD28 activation.
1015 Tconv cells were loaded with Fluo-4 AM, and left in steady state without anti-CD3 and anti-CD28
1016 stimulation, or treated with anti-CD3 and anti-CD28 stimulation to record SOCE signal.
1017 Fluorescence was recorded with the interval of 10 s. Left, the F/F0 of mean fluorescence
1018 intensities were calculated and presented, Right, graph for standard deviation of fluorescence in
1019 these cells. n>50, N=3.

1020 B. tTreg and iTreg cells was sorted and restimulated with various concentrations of anti-CD3 and
1021 anti-CD28 antibodies. The percentage of $Foxp3^+$ cells was analyzed by intracellular staining after
1022 2d restimulation. n=3, N=3.

1023 C. Early TCR signal of pCD3ζ in tTreg and iTreg after TCR cross-linking. Sorted iTreg, tTreg and
1024 Tconv cells were mixed and stained with biotin-anti-CD3 and biotin anti-CD28 for 1 h. TCR
1025 crosslink was perform by the addition of streptavidin. Cells were fixed at the indicated times and
1026 stained with pCD3ζ Y142 antibody. Left, representative flow overlays for pCD3ζ Y142 in rest and
1027 activated cells. Right, graph for the MFI changes in activated cells after indicated time.

1028 D. Foxp3-RFP^+ iTreg were stimulated by anti-CD3 and anti-CD28, after the indicated times, cells
1029 were collected and the cytoplasmic/Nuclear component were separated. The cytoplasmic and
1030 nuclear NFATc1 and NFATc2 were analyzed by western blot. Actin and GAPDH were used as
1031 loading control of cytoplasmic protein, and Lamin A/C as nuclear. N=3.

1032 E. Foxp3-RFP^+ tTregs were stimulated by anti-CD3 and anti-CD28, after 1h ionomycin and TG were
1033 added in the culture medium. After 24h of stimulation, the percentages of live cells in $CD4^+$ cells
1034 were monitored. N=3.

1035 Here, **, $P < 0.01$, by students's t test.

1036

1037

1038 **Fig S3. iTreg has highest proliferation state and partial Treg feature**

1039 A. Left, heatmap showing the top genes that positively contribute to PC1. Right, heatmap showing
1040 the top genes that negatively contribute to PC1. As shown, genes contributing positively to PC1
1041 mainly belong to proliferation such as nuclear division, DNA replication and cell cycle, while
1042 the negatively associated ones mainly belong to chromatin state regulations such as
1043 histone/DNA modification.

1044 B. Left, heatmap showing the top genes that positively contribute to PC2. Right, heatmap showing
1045 the top genes that negatively contribute to PC2. As shown, the main contributors to PC2 axis were
1046 the signature genes of Tconvs and Tregs, such as Ifng, Il17ra, T-bet in the positive direction,
1047 Foxp3, Ctla4, Tnfrsf9 in the negative direction.

1048 C. Heatmap showing the expression of cell type specifically expressed genes in RNA-Seq data. As
1049 shown, four major groups of genes were identified, based on the significant higher expression in
1050 specific cell types. Different group of genes were labeled.

1051 D. Heatmap showing the chromatin accessibility of tTreg specifically accessible peaks in tTreg
1052 specifically expressed genes.

1053 E. Genomic track showing chromatin accessibility of Irf4, Atf3, Lta, Tnfsf8, Tnfsf4, Tnsfsf14,
1054 Il12rb2, Il9, Gzmc in activated Tconv and iTreg.

1055

1056

1057 **Fig S4. SOCE signaling and NFAT cause instability and downregulate Treg related gene**

1058 A. Stability of iTreg treated with CM-4620, CsA and BTP-2 upon restimulation. iTregs were
1059 restimulated by anti-CD3 and CD28 in the presence of CsA, CM-4620 and BTP-2. Percentages of
1060 Foxp3+ cells were analyzed by intracellular staining after 2 d restimulation. Left, representative
1061 histograms. Right, graph for the percentages of Foxp3. n=3, N=3.

1062 B. Stability of ionomycin and CsA treated iTreg. iTreg were treated with ionomycin and CsA,
1063 percentages of Foxp3+ cells were analyzed by intracellular staining after 1 d restimulation. n=3,
1064 N=3.

1065 C. Stability of NF-kb and c-Jun/c-Fos inhibitor treated iTreg. Sorted Foxp3-GFP+ iTregs were rested
1066 for 1d, then restimulated by anti-CD3 and CD28 in the presence of indicated inhibitors.
1067 Percentages of Foxp3+ cells were analyzed by intracellular staining after 2d restimulation. n=3.

1068 D. Representative genes downregulated after iTreg restimulation rescued by inhibiting Calcium or
1069 NFAT.

1070 E. Biological terms enriched by the significant downregulated genes after iTreg restimulation
1071 rescued by inhibiting Calcium or NFAT.
1072 Here, *, $P < 0.05$; **, $P < 0.01$, ***, $P < 0.001$, ****, $P < 0.0001$, by students's t test.
1073
1074
1075 **Fig S5. iTregs have highest accessibility in T_H-associated genes**
1076 A. Sorted Foxp3-RFP$^+$ naïve Tconvs were induced into iTregs in the presence of IL-2 and TGF-β for
1077 4 days, on the second day and third day, iTreg cells were infected with retrovirus packaging with
1078 NFAT-flag plasmid. The infected Foxp3-RFP$^+$ iTregs were sorted and restimulated by anti-CD3
1079 and CD28 for 1d. after 1d stimulation, the cells were collected and performed Cut&Tag assay.
1080 B. Genome track visualization of chromatin accessibility profiles in typical genes Il21, Il12rb2, and
1081 Tbx21.
1082 C. The genomic distribution of Cut&Tag peaks for NFAT in rest iTregs and restimulated iTregs.
1083 D. Normalized counts of NFAT Cut&Tag reads in resting and restimulated iTreg, centered on the TSS
1084 region NFAT-downregulated Treg genes.
1085
1086
1087 **Fig S6. Different optimization of iTreg have various impact on activation region and Treg region**
1088 A. Line plots (top) and heatmaps (bottom) of activation regions in anti-CD3, anti-CD28, IL-2 and
1089 TGF-β induced iTregs, treated with Retinoic acid, Rapamycin, Vitamin C, removal of CD28, and
1090 AS2863619.
1091 B. Line plots (top) and heatmaps (bottom) of Treg regions in anti-CD3, anti-CD28, IL-2 and TGF-β
1092 induced iTregs, treated with Retinoic acid, Rapamycin, Vitamin C, removal of CD28, and
1093 AS2863619.
1094
1095
1096 **Movie 1-3. Imaging of SOCE signal in Tconvs, tTregs and iTregs.**
1097 Tconvs (Movie 1), tTregs (Movie 2) and iTregs (Movie 3) were sorted and resting for 1d, then cells
1098 were loaded with Fluo-4 AM and activated by anti-CD3 and anti-CD28 in confocal dish. After
1099 activation for 50 min, movies were recorded for total 600 s with the interval of 10 s.

Figure 1

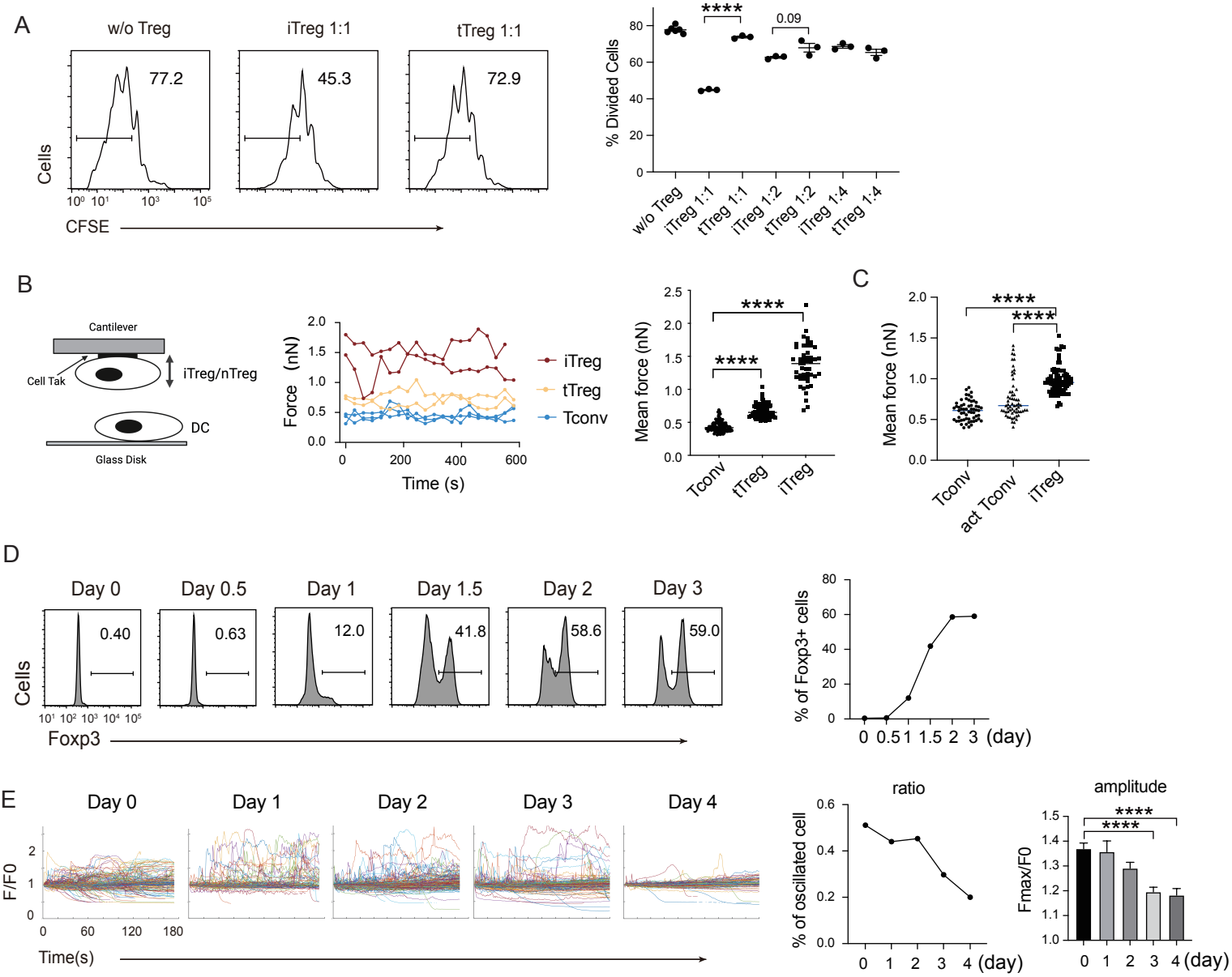
A
w/o Treg
iTreg 1:1
tTreg 1:1
77.2
45.3
72.9
Cells
CFSE
% Divided Cells
****
0.09
w/o Treg
iTreg 1:1
tTreg 1:1
iTreg 1:2
tTreg 1:2
iTreg 1:4
tTreg 1:4
B
Cantilever
Cell Tak
iTreg/nTreg
DC
Glass Disk
Force (nN)
Time (s)
iTreg
tTreg
Tconv
Mean force (nN)
****
****
Tconv
tTreg
iTreg
C
Mean force (nN)
****
****
Tconv
act Tconv
iTreg
D
Day 0
Day 0.5
Day 1
Day 1.5
Day 2
Day 3
0.40
0.63
12.0
41.8
58.6
59.0
Cells
Foxp3
% of Foxp3+ cells
(day)
E
Day 0
Day 1
Day 2
Day 3
Day 4
F/F0
Time(s)
ratio
% of oscillated cell
(day)
amplitude
Fmax/F0
****
****
(day)

Figure 2

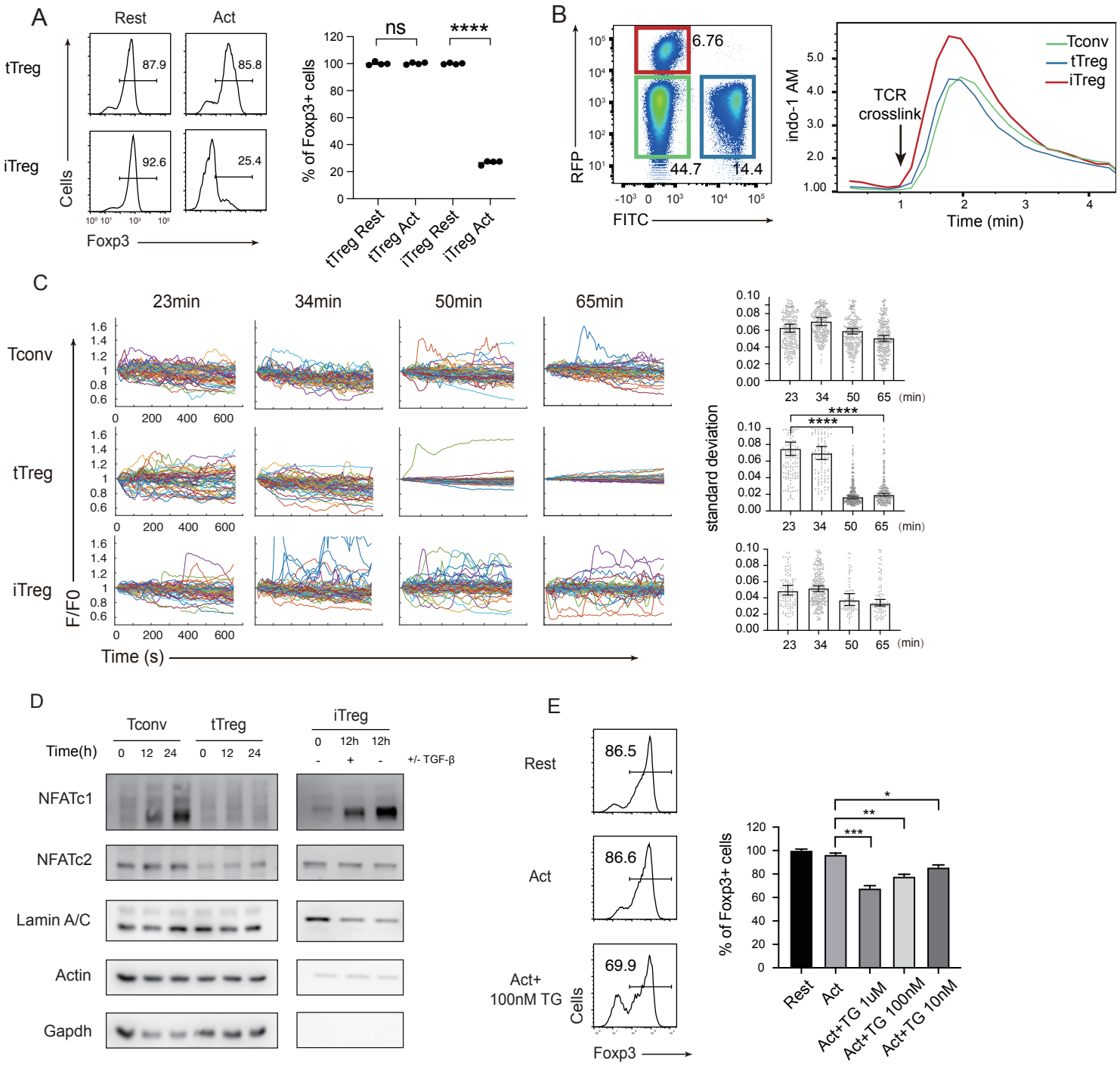
A
Rest
Act
tTreg
iTreg
87.9
85.8
92.6
25.4
Cells
Foxp3
ns
****
% of Foxp3+ cells
tTreg Rest
tTreg Act
iTreg Rest
iTreg Act
B
6.76
44.7
14.4
RFP
FITC
indo-1 AM
TCR crosslink
Tconv
tTreg
iTreg
Time (min)
C
23min
34min
50min
65min
Tconv
tTreg
iTreg
F/F0
Time (s)
standard deviation
(min)
D
Tconv
tTreg
iTreg
Time(h)
0 12 24
0 12 24
0 12h 12h
- + -
+/- TGF-β
NFATc1
NFATc2
Lamin A/C
Actin
Gapdh
E
Rest
Act
Act+ 100nM TG
86.5
86.6
69.9
Cells
Foxp3
% of Foxp3+ cells
***
**
*
Rest
Act
Act+TG 1uM
Act+TG 100nM
Act+TG 10nM

Figure 3

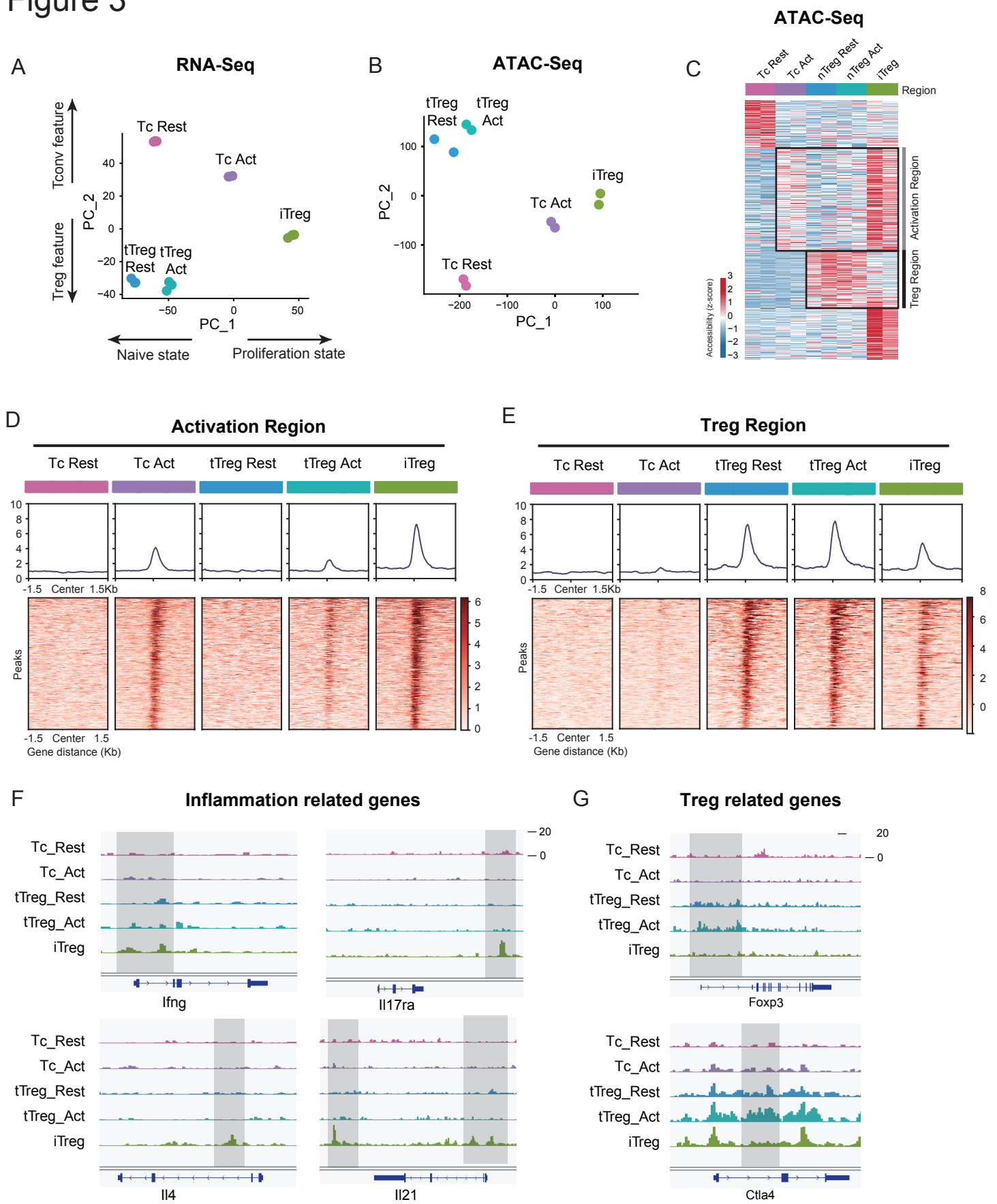
A
RNA-Seq
Tconv feature
Treg feature
Tc Rest
Tc Act
iTreg
tTreg Rest
tTreg Act
PC_2
PC_1
Naive state
Proliferation state
B
ATAC-Seq
tTreg Rest
tTreg Act
iTreg
Tc Act
Tc Rest
PC_2
PC_1
C
ATAC-Seq
Tc Rest
Tc Act
nTreg Rest
nTreg Act
iTreg
Region
Activation Region
Treg Region
Accessibility (z-score)
D
Activation Region
Tc Rest
Tc Act
tTreg Rest
tTreg Act
iTreg
-1.5 Center 1.5Kb
Peaks
-1.5 Center 1.5
Gene distance (Kb)
E
Treg Region
Tc Rest
Tc Act
tTreg Rest
tTreg Act
iTreg
-1.5 Center 1.5Kb
Peaks
-1.5 Center 1.5
Gene distance (Kb)
F
Inflammation related genes
Tc_Rest
Tc_Act
tTreg_Rest
tTreg_Act
iTreg
Ifng
Il17ra
Il4
Il21
G
Treg related genes
Tc_Rest
Tc_Act
tTreg_Rest
tTreg_Act
iTreg
Foxp3
Ctla4

Figure 4

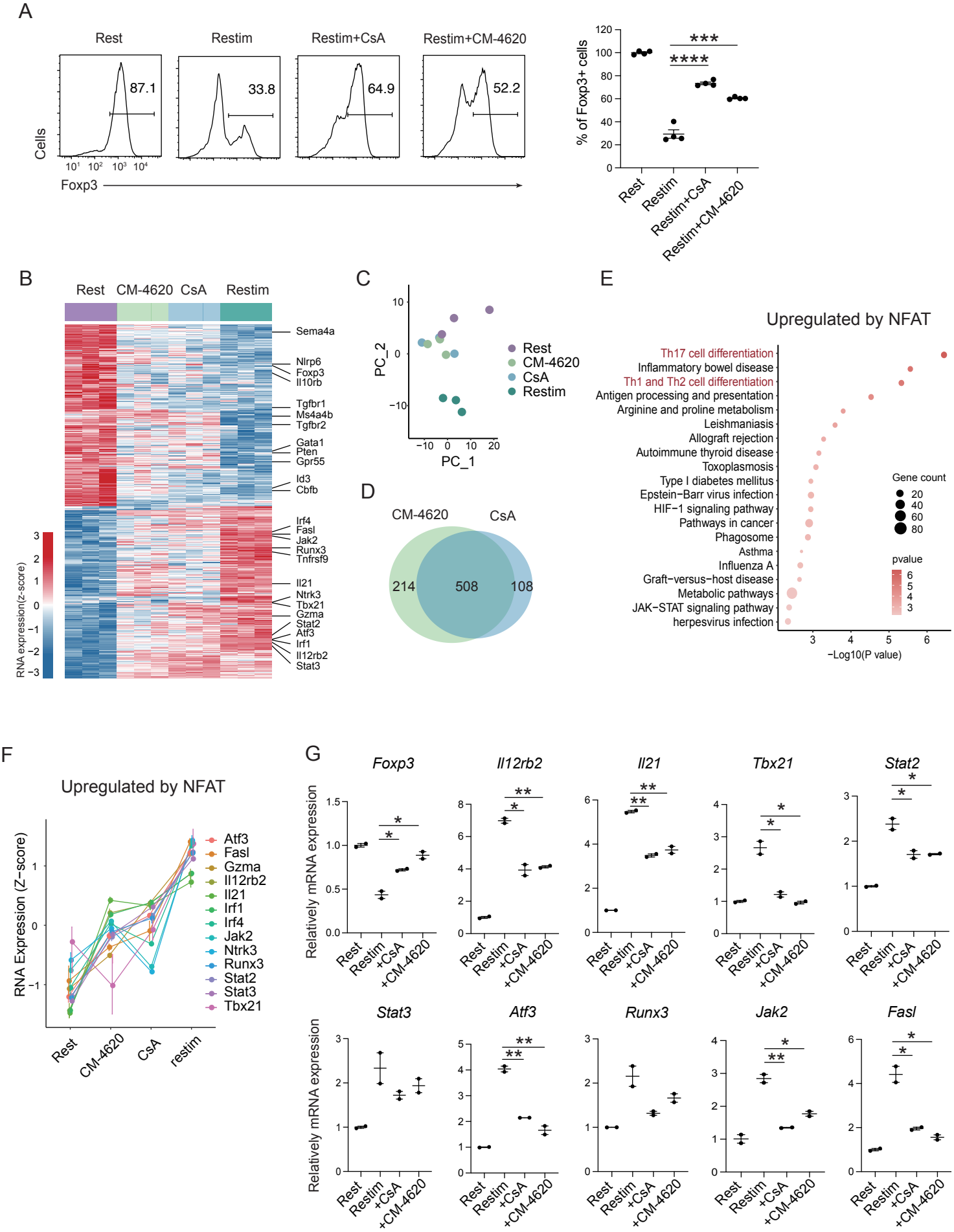
A
Rest
Restim
Restim+CsA
Restim+CM-4620
87.1
33.8
64.9
52.2
Cells
Foxp3
% of Foxp3+ cells
***
****
B
Rest CM-4620 CsA Restim
Sema4a
Nlrp6
Foxp3
Il10rb
Tgfbr1
Ms4a4b
Tgfbr2
Gata1
Pten
Gpr55
Id3
Cbfb
Irf4
Fasl
Jak2
Runx3
Tnfrsf9
Il21
Ntrk3
Tbx21
Gzma
Stat2
Atf3
Irf1
Il12rb2
Stat3
RNA expression(z-score)
C
PC_2
PC_1
Rest
CM-4620
CsA
Restim
D
CM-4620
CsA
214
508
108
E
Upregulated by NFAT
Th17 cell differentiation
Inflammatory bowel disease
Th1 and Th2 cell differentiation
Antigen processing and presentation
Arginine and proline metabolism
Leishmaniasis
Allograft rejection
Autoimmune thyroid disease
Toxoplasmosis
Type I diabetes mellitus
Epstein−Barr virus infection
HIF−1 signaling pathway
Pathways in cancer
Phagosome
Asthma
Influenza A
Graft−versus−host disease
Metabolic pathways
JAK−STAT signaling pathway
herpesvirus infection
Gene count
pvalue
−Log10(P value)
F
Upregulated by NFAT
RNA Expression (Z−score)
Atf3
Fasl
Gzma
Il12rb2
Il21
Irf1
Irf4
Jak2
Ntrk3
Runx3
Stat2
Stat3
Tbx21
Rest
CM-4620
CsA
restim
G
Foxp3
Il12rb2
Il21
Tbx21
Stat2
Stat3
Atf3
Runx3
Jak2
Fasl
Relatively mRNA expression
Rest
Restim
+CsA
+CM-4620

Figure 5

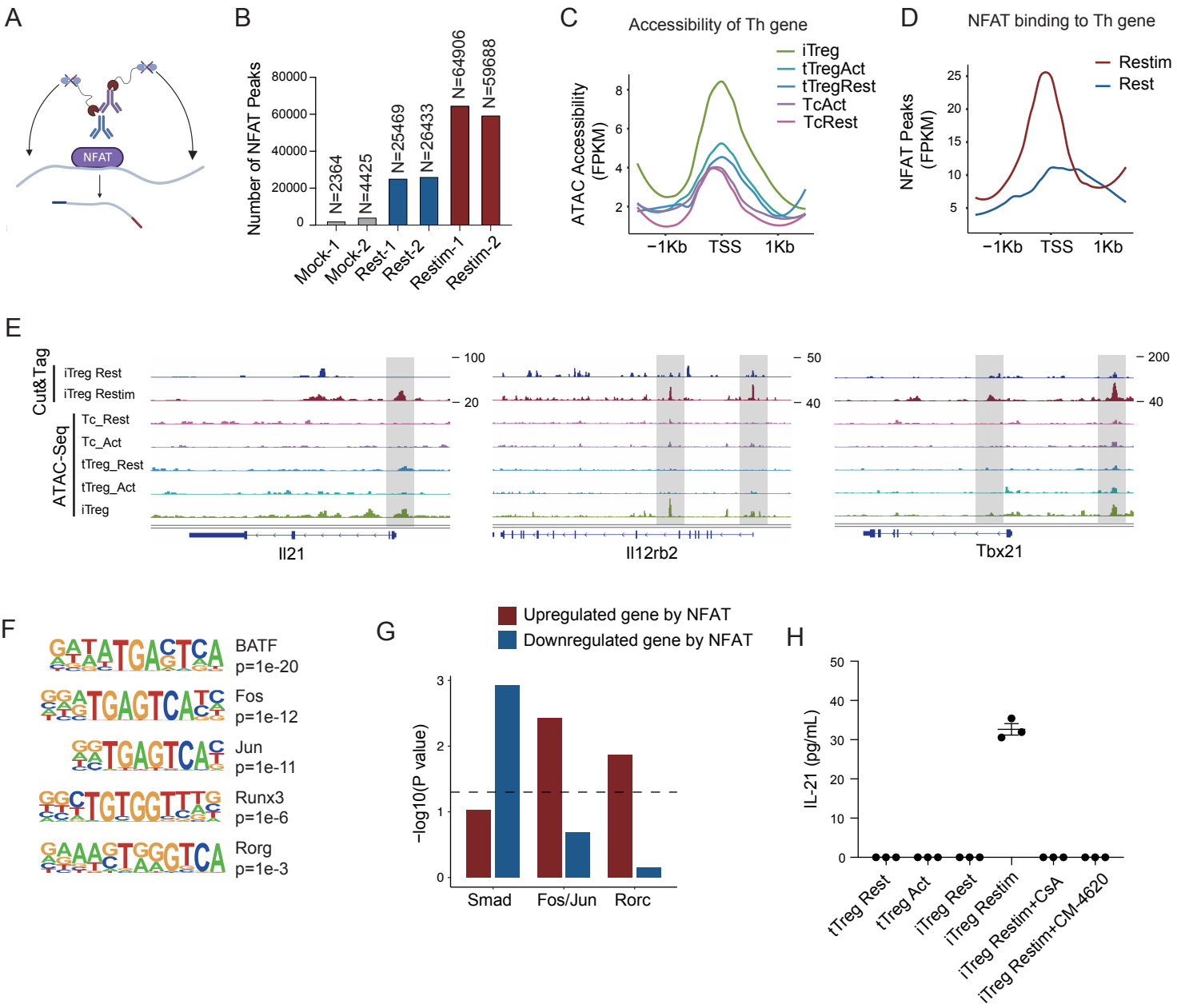
A
NFAT
B
Number of NFAT Peaks
80000
60000
40000
20000
0
N=2364
N=4425
N=25469
N=26433
N=64906
N=59688
Mock-1
Mock-2
Rest-1
Rest-2
Restim-1
Restim-2
C
Accessibility of Th gene
iTreg
tTregAct
tTregRest
TcAct
TcRest
ATAC Accessibility (FPKM)
8
6
4
2
−1Kb
TSS
1Kb
D
NFAT binding to Th gene
Restim
Rest
NFAT Peaks (FPKM)
25
20
15
10
5
−1Kb
TSS
1Kb
E
Cut&Tag
iTreg Rest
iTreg Restim
ATAC-Seq
Tc_Rest
Tc_Act
tTreg_Rest
tTreg_Act
iTreg
100
20
50
40
200
40
Il21
Il12rb2
Tbx21
F
BATF
p=1e-20
Fos
p=1e-12
Jun
p=1e-11
Runx3
p=1e-6
Rorg
p=1e-3
G
Upregulated gene by NFAT
Downregulated gene by NFAT
−log10(P value)
3
2
1
0
Smad
Fos/Jun
Rorc
H
IL-21 (pg/mL)
50
40
30
20
10
0
tTreg Rest
tTreg Act
iTreg Rest
iTreg Restim
iTreg Restim+CsA
iTreg Restim+CM-4620

Figure 6

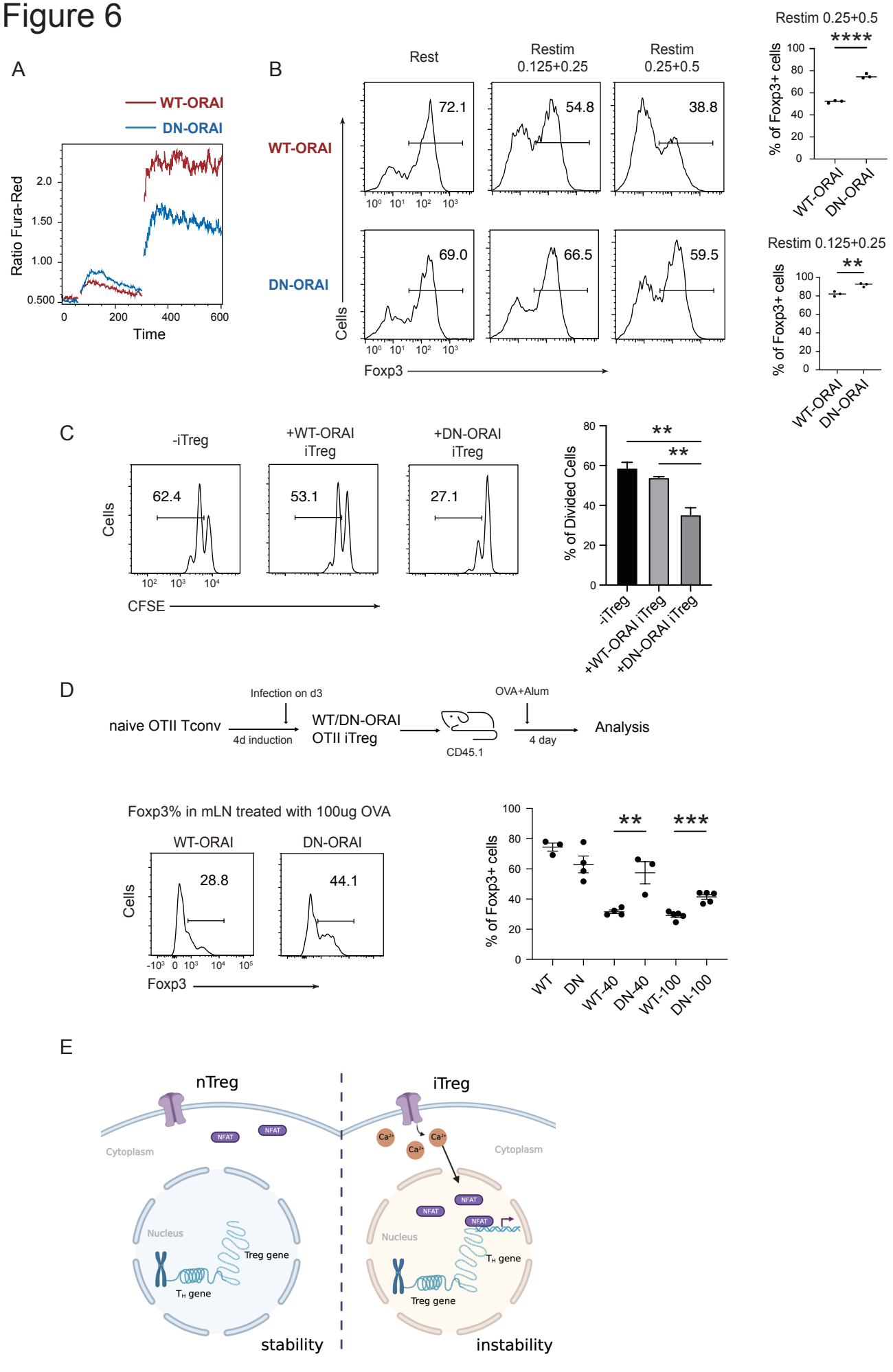
A
WT-ORAI
DN-ORAI
Ratio Fura-Red
2.0
1.50
1.00
0.500
0
200
400
600
Time
B
Rest
Restim 0.125+0.25
Restim 0.25+0.5
WT-ORAI
DN-ORAI
72.1
54.8
38.8
69.0
66.5
59.5
Cells
Foxp3
Restim 0.25+0.5
****
% of Foxp3+ cells
WT-ORAI
DN-ORAI
Restim 0.125+0.25
**
C
-iTreg
+WT-ORAI iTreg
+DN-ORAI iTreg
62.4
53.1
27.1
Cells
CFSE
% of Divided Cells
**
**
-iTreg
+WT-ORAI iTreg
+DN-ORAI iTreg
D
naive OTII Tconv
Infection on d3
4d induction
WT/DN-ORAI OTII iTreg
CD45.1
OVA+Alum
4 day
Analysis
Foxp3% in mLN treated with 100ug OVA
WT-ORAI
DN-ORAI
28.8
44.1
Cells
Foxp3
% of Foxp3+ cells
**
***
WT
DN
WT-40
DN-40
WT-100
DN-100
E
nTreg
iTreg
Cytoplasm
NFAT
Nucleus
Treg gene
TH gene
Ca2+
stability
instability

Figure S1

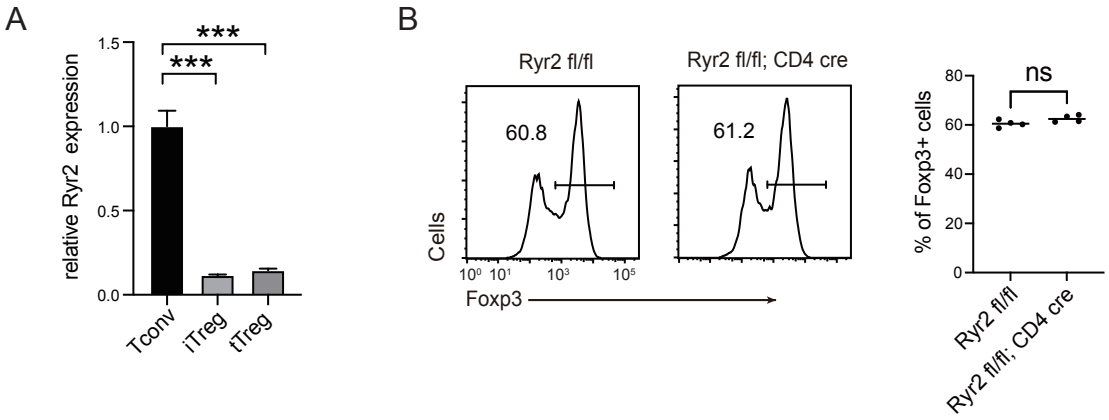
A
***
***
1.5
1.0
0.5
0.0
relative Ryr2 expression
Tconv
iTreg
tTreg
B
Ryr2 fl/fl
Ryr2 fl/fl; CD4 cre
60.8
61.2
Cells
Foxp3
ns
80
60
40
20
0
% of Foxp3+ cells
Ryr2 fl/fl
Ryr2 fl/fl; CD4 cre

Figure S2

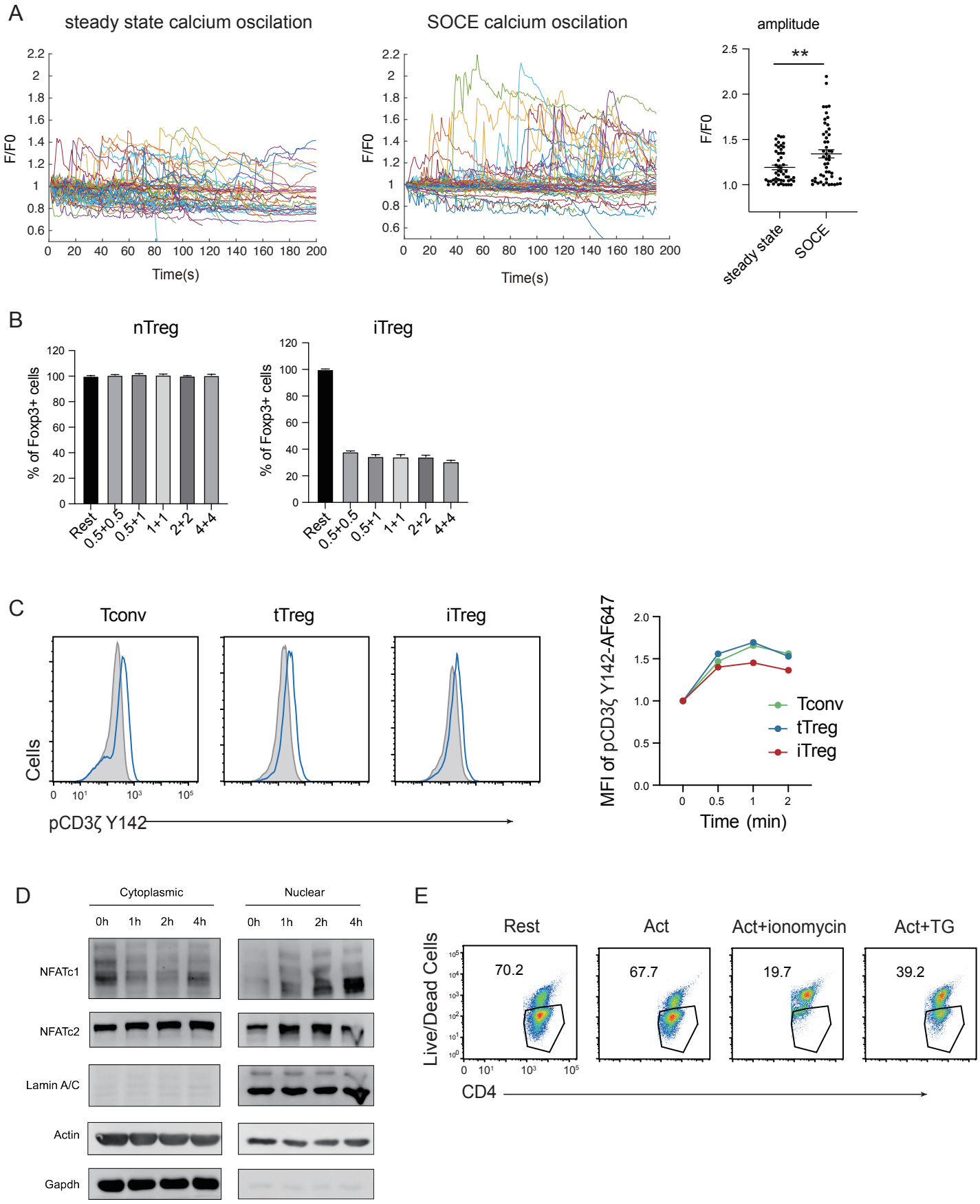
A
steady state calcium oscilation
SOCE calcium oscilation
amplitude
F/F0
Time(s)
**
steady state
SOCE
B
nTreg
iTreg
% of Foxp3+ cells
Rest
0.5+0.5
0.5+1
1+1
2+2
4+4
C
Tconv
tTreg
iTreg
Cells
pCD3ζ Y142
MFI of pCD3ζ Y142-AF647
Time (min)
D
Cytoplasmic
Nuclear
0h
1h
2h
4h
NFATc1
NFATc2
Lamin A/C
Actin
Gapdh
E
Rest
Act
Act+ionomycin
Act+TG
Live/Dead Cells
CD4
70.2
67.7
19.7
39.2

Figure S3

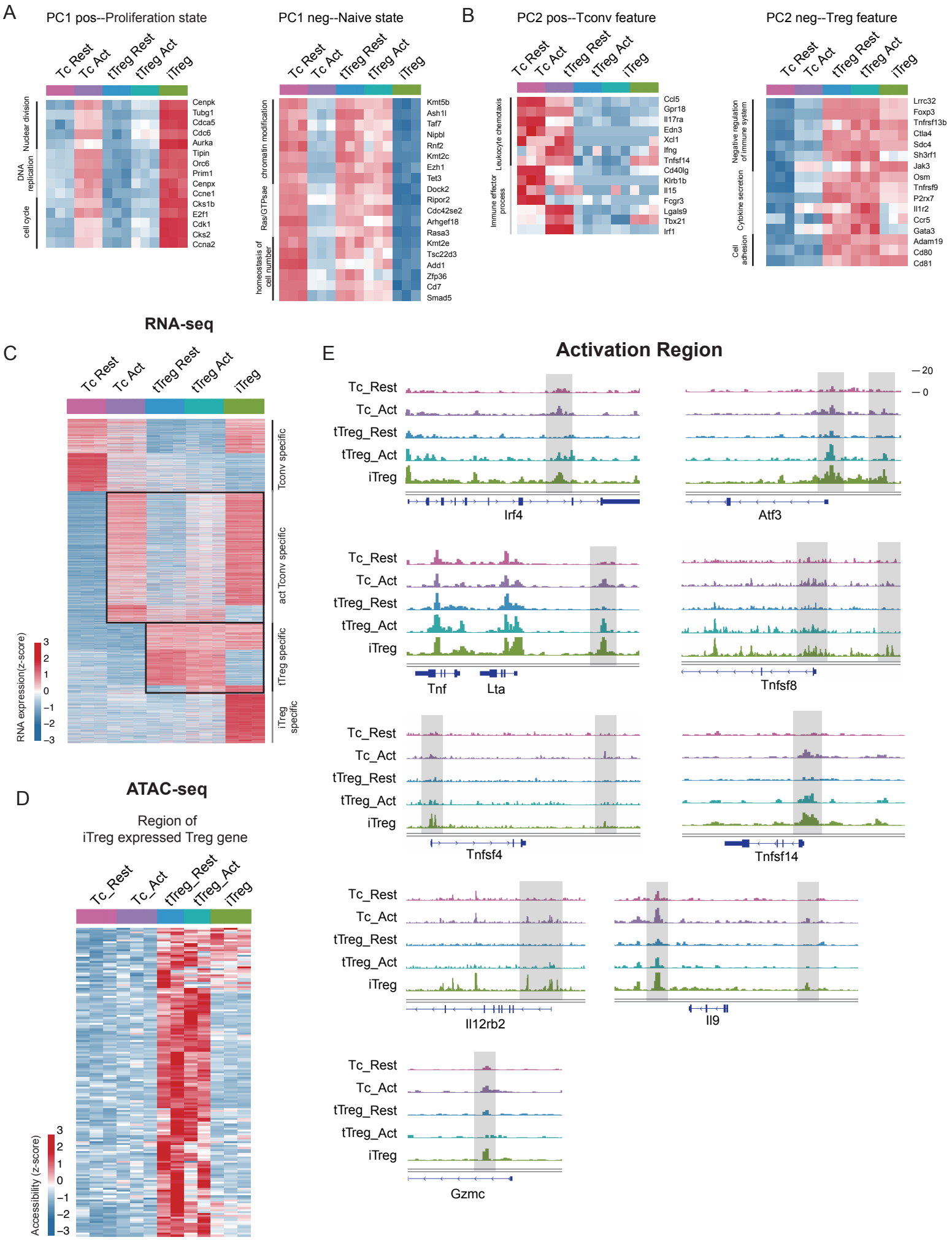
A
PC1 pos--Proliferation state
PC1 neg--Naive state
Tc Rest
Tc Act
tTreg Rest
tTreg Act
iTreg
Nuclear division
DNA replication
cell cycle
Cenpk
Tubg1
Cdca5
Cdc6
Aurka
Tipin
Orc6
Prim1
Cenpx
Ccne1
Cks1b
E2f1
Cdk1
Cks2
Ccna2
chromatin modification
Ras/GTPsae
homeostasis of cell number
Kmt5b
Ash1l
Taf7
Nipbl
Rnf2
Kmt2c
Ezh1
Tet3
Dock2
Ripor2
Cdc42se2
Arhgef18
Rasa3
Kmt2e
Tsc22d3
Add1
Zfp36
Cd7
Smad5
B
PC2 pos--Tconv feature
PC2 neg--Treg feature
Leukocyte chemotaxis
Immune effector process
Ccl5
Gpr18
Il17ra
Edn3
Xcl1
Ifng
Tnfsf14
Cd40lg
Klrb1b
Il15
Fcgr3
Lgals9
Tbx21
Irf1
Negative regulation of immune system
Cytokine secretion
Cell adhesion
Lrrc32
Foxp3
Tnfrsf13b
Ctla4
Sdc4
Sh3rf1
Jak3
Osm
Tnfrsf9
P2rx7
Il1r2
Ccr5
Gata3
Adam19
Cd80
Cd81
RNA-seq
C
Tc Rest
Tc Act
tTreg Rest
tTreg Act
iTreg
Tconv specific
act Tconv specific
tTreg specific
iTreg specific
RNA expression(z-score)
3
2
1
0
−1
−2
−3
ATAC-seq
D
Region of
iTreg expressed Treg gene
Tc_Rest
Tc_Act
tTreg_Rest
tTreg_Act
iTreg
Accessibility (z-score)
3
2
1
0
−1
−2
−3
Activation Region
E
Tc_Rest
Tc_Act
tTreg_Rest
tTreg_Act
iTreg
20
0
Irf4
Atf3
Tnf
Lta
Tnfsf8
Tnfsf4
Tnfsf14
Il12rb2
Il9
Gzmc

Figure S4

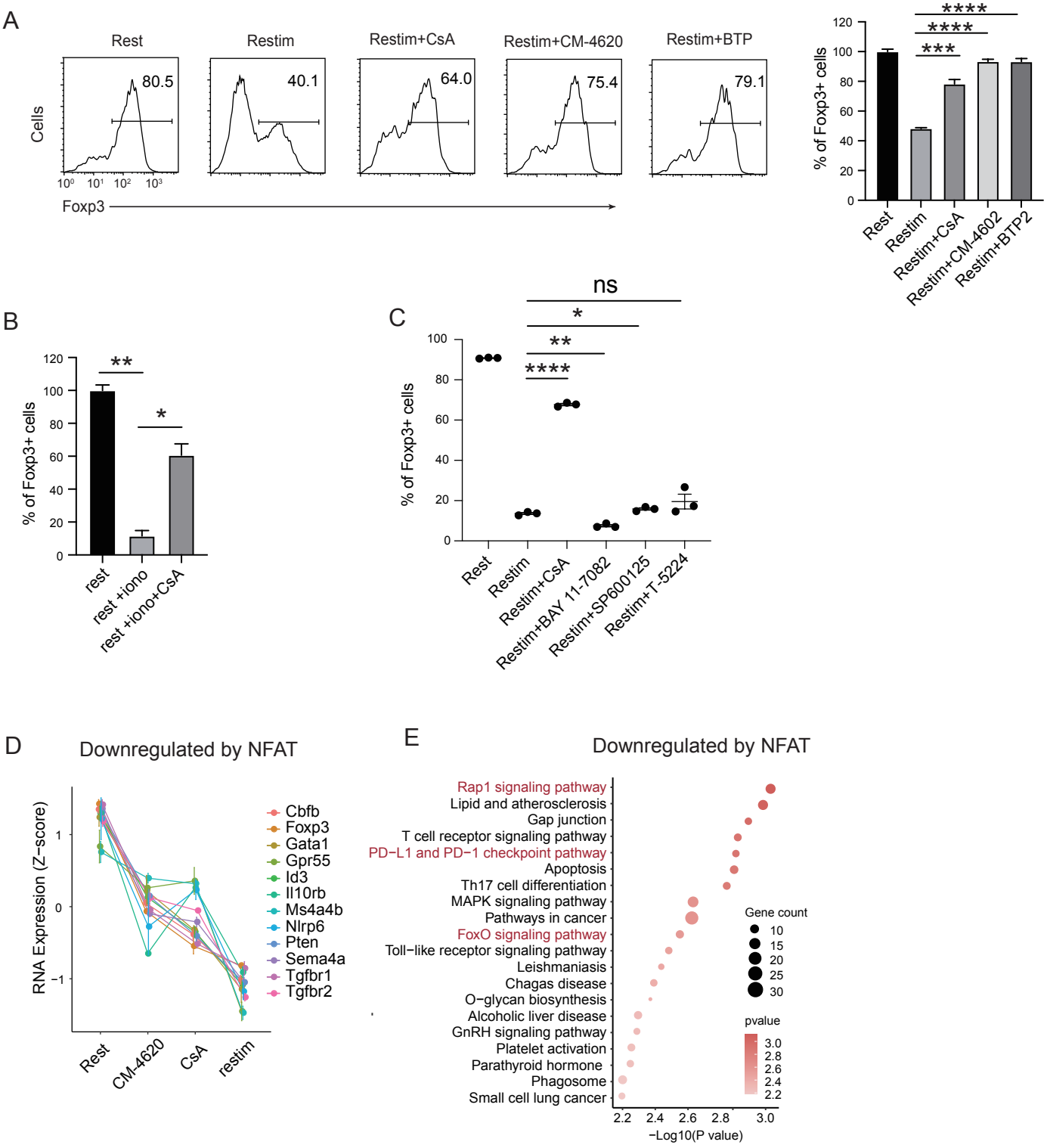
A
Rest
Restim
Restim+CsA
Restim+CM-4620
Restim+BTP
80.5
40.1
64.0
75.4
79.1
Cells
Foxp3
% of Foxp3+ cells
Rest
Restim
Restim+CsA
Restim+CM-4602
Restim+BTP2
B
% of Foxp3+ cells
rest
rest +iono
rest +iono+CsA
C
ns
% of Foxp3+ cells
Rest
Restim
Restim+CsA
Restim+BAY 11-7082
Restim+SP600125
Restim+T-5224
D
Downregulated by NFAT
RNA Expression (Z−score)
Cbfb
Foxp3
Gata1
Gpr55
Id3
Il10rb
Ms4a4b
Nlrp6
Pten
Sema4a
Tgfbr1
Tgfbr2
Rest
CM-4620
CsA
restim
E
Downregulated by NFAT
Rap1 signaling pathway
Lipid and atherosclerosis
Gap junction
T cell receptor signaling pathway
PD−L1 and PD−1 checkpoint pathway
Apoptosis
Th17 cell differentiation
MAPK signaling pathway
Pathways in cancer
FoxO signaling pathway
Toll−like receptor signaling pathway
Leishmaniasis
Chagas disease
O−glycan biosynthesis
Alcoholic liver disease
GnRH signaling pathway
Platelet activation
Parathyroid hormone
Phagosome
Small cell lung cancer
Gene count
pvalue
−Log10(P value)

Figure S5

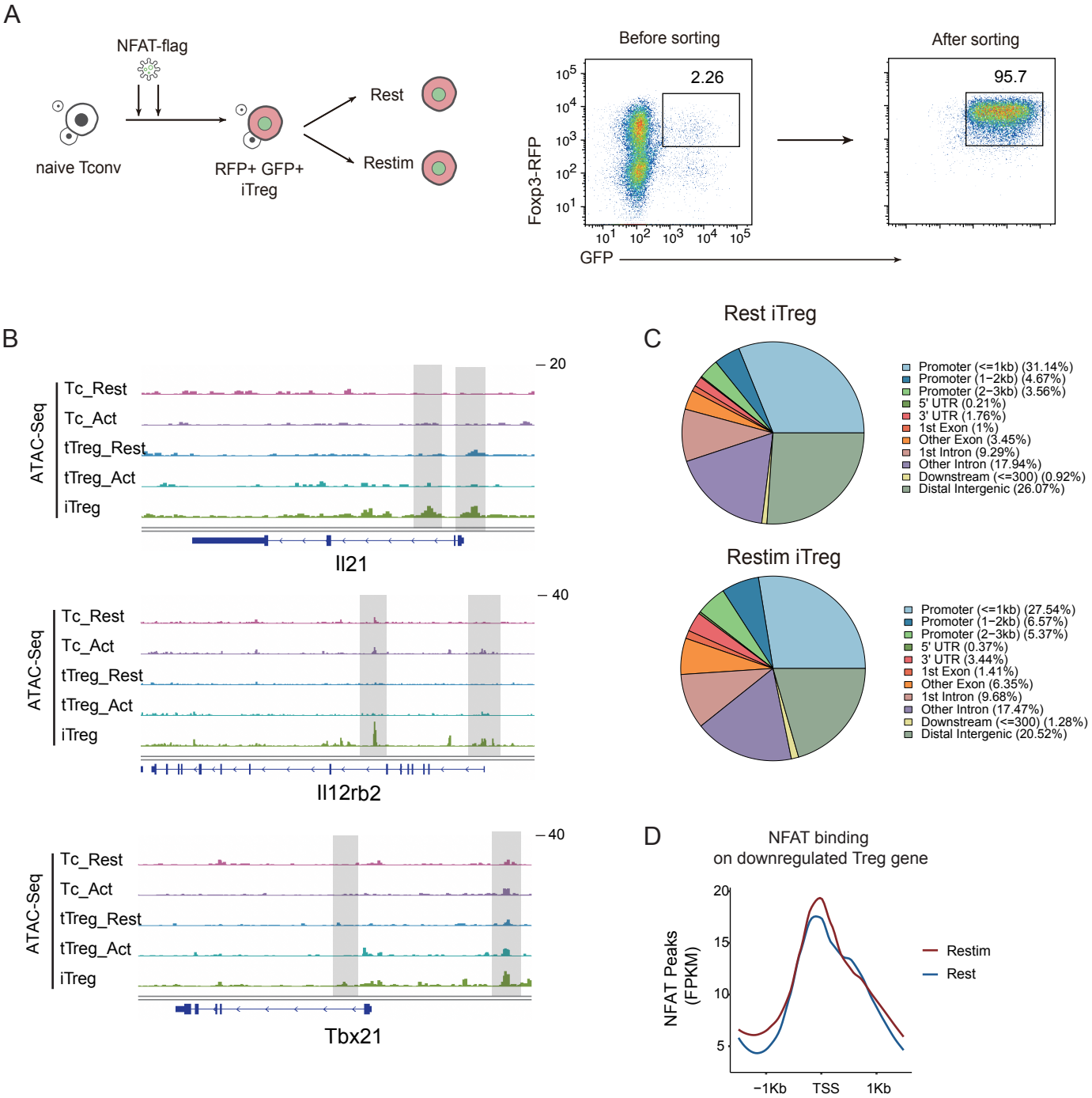
A
NFAT-flag
naive Tconv
RFP+ GFP+
iTreg
Rest
Restim
Before sorting
After sorting
2.26
95.7
Foxp3-RFP
GFP
B
ATAC-Seq
Tc_Rest
Tc_Act
tTreg_Rest
tTreg_Act
iTreg
Il21
Il12rb2
Tbx21
C
Rest iTreg
Promoter (<=1kb) (31.14%)
Promoter (1−2kb) (4.67%)
Promoter (2−3kb) (3.56%)
5' UTR (0.21%)
3' UTR (1.76%)
1st Exon (1%)
Other Exon (3.45%)
1st Intron (9.29%)
Other Intron (17.94%)
Downstream (<=300) (0.92%)
Distal Intergenic (26.07%)
Restim iTreg
Promoter (<=1kb) (27.54%)
Promoter (1−2kb) (6.57%)
Promoter (2−3kb) (5.37%)
5' UTR (0.37%)
3' UTR (3.44%)
1st Exon (1.41%)
Other Exon (6.35%)
1st Intron (9.68%)
Other Intron (17.47%)
Downstream (<=300) (1.28%)
Distal Intergenic (20.52%)
D
NFAT binding
on downregulated Treg gene
NFAT Peaks
(FPKM)
Restim
Rest
−1Kb
TSS
1Kb

Figure S6

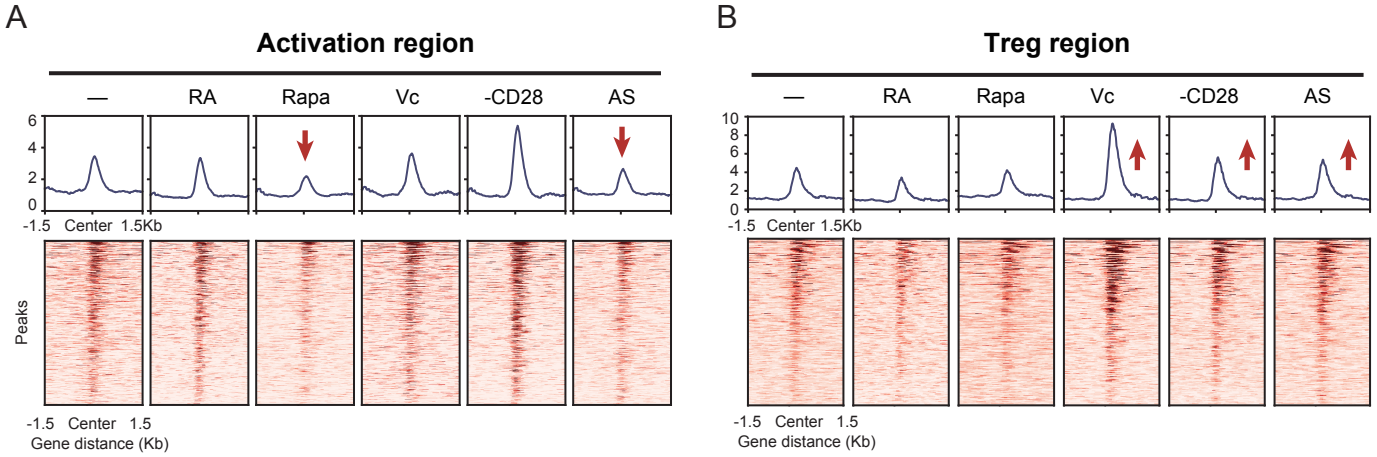
A
Activation region
—
RA
Rapa
Vc
-CD28
AS
6
4
2
0
-1.5 Center 1.5Kb
Peaks
-1.5 Center 1.5
Gene distance (Kb)
B
Treg region
—
RA
Rapa
Vc
-CD28
AS
10
8
6
4
2
0
-1.5 Center 1.5Kb
-1.5 Center 1.5
Gene distance (Kb)